Journal of Minerals and Materials Characterization and Engineering, 2022, 10, 287-318
https://www.scirp.org/journal/jmmce
ISSN Online: 2327-4085
ISSN Print: 2327-4077

Mineralogy, Petrography and Geochemistry of the Ina Syenite (Linté, Central Cameroon) as a Source of Industrial Feldspars

Soualiou Njimbouombouo Mouliom[1,2,3*], André Njoya[4], Rose Yongue Fouateu[2], Nguo Silvestre Kanouo[5], Daniel Lamilen Mbila[2], Bernard Charlier[1], Nathalie Fagel[1]

[1]Département de Géologie, Université de Liège, Liège, Belgique
[2]Département des Géosciences, Université de Yaoundé I, Yaoundé Cameroun
[3]Mission de Promotion des Matériaux Locaux, Yaoundé, Cameroun
[4]Institut des beaux-arts, Université de Dschang, Foumban, Cameroun
[5]Mineral Exploration and Ore Genesis Unit, Department of Mining Engineering and Mineral Processing, Faculty of Mines and Petroleum Industries, University of Maroua, Maroua, Cameroon
Email: *njimbouombouomouliom@yahoo.fr

How to cite this paper: Mouliom, S.N., Njoya, A., Fouateu, R.Y., Kanouo, N.S., Mbila, D.L., Charlier, B. and Fagel, N. (2022) Mineralogy, Petrography and Geochemistry of the Ina Syenite (Linté, Central Cameroon) as a Source of Industrial Feldspars. *Journal of Minerals and Materials Characterization and Engineering*, **10**, 287-318.
https://doi.org/10.4236/jmmce.2022.103022

Received: March 31, 2022
Accepted: May 28, 2022
Published: May 31, 2022

Abstract

The syenite from Ina (Central region of Cameroon) constitutes a 1000 km² syntectonic batholith intruded in the Paleoproterozoic granitic basement. The aim of this work is to assess the potential of the Ina batholith syenite as a feldspar minerals resource for industrial use through petrographic and geochemical characterization. Most of the rocks are grey coloured and consist of shimmering feldspar phenocrysts in a fine-grained ferromagnesian matrix. Petrography reveals the presence of two major syenite facies: a widely distributed porphyritic syenite and a less-abundant massive syenite. These facies are dominated by phenocrysts of sub-automorphic perthitic orthoclase. Its malgachite face is due to the presence of numerous inclusions of opaque minerals observed by scanning electron microscopy (ESEM-EDX). Plagioclase phenocrysts have a zonal texture characterised microscopically by an oscillatory compositional zonation. Biotite, hornblende and augite, identified by X-ray powder diffraction, are finely disseminated in the feldspar matrix. Quartz appears as small automorphic crystals with maximum abundance of about 4 wt%. The XRF chemical composition reveals, alongside silica (59.29 wt% to 63.27 wt%), significant proportion of alumina (15.82 wt% to 19.80 wt%), potassium and sodium oxides considered as fluxing elements (K_2O + $Na_2O \geq 10$ wt%). The K_2O/Na_2O ratio varies between 1.65 and 5.51 (average 2.58). Iron and titanium oxides ($1 \geq$ wt% $Fe_2O_3 + TiO_2 \geq 5$), harmful in ceramic industry, are high as in most other feldspathic sources. The characteristics of the Ina syenite are close to most of the syenite ores used worldwide for

ceramics and glass raw materials and necessitates purification and beneficiation treatments. Others rock types have been identified at the study site (granite, monzonite, granodiorite) and are considered as inappropriate as a source of industrial feldspars.

Keywords

Ina Syenite, Petrography, Mineralogy, Feldspathic Fluxes

1. Introduction

Syenites are leucocratic to mesocratic felsic igneous rocks belonging to intermediate plutonic rocks with trachyte as the volcanic equivalent. These rocks are present in most tectonic contexts except in mid-ocean [1]. They are formed by the cooling of a crustal or mantellic magma saturated or undersaturated with silica and outcrop as allochthonous (batholith), dyke or vein within the granite massif that it intersects [2] [3] [4] [5]. Syenites display coarse grain texture, porphyritic texture or sometimes pegmatitic texture. They are essentially composed of alkaline feldspars (content ≥ 75%), in particular orthoclase and microcline and often sodium plagioclase (around 15%). Apart from feldspars, the rock contains quartz, mafic minerals such as biotite, pyroxene and amphiboles. Magnetite, ilmenite, apatite and titanite constitute the accessory phases [6].

The geological characteristics of syenites and their deposits make them an industrial mineral exploited for economic and strategic purposes worldwide. In the field of civil engineering, syenite has long been exploited as freestone [6] [7] [8]; in agriculture as a source of potash for soil enrichment [9] [10] [11]. Gold mineralization and rare earth elements are also exploited in some syenites [12] [13] [14] [15] [16]. They are also used as filler in the paint industries [17]. Syenite is exploited as an alternative source of feldspathic flux for the ceramic and glass industry [3] [6] [10] [17]-[24]. Feldspars are mainly mined in albitites, aplites and pegmatites [17] [22]. However, these deposits are being depleted at a tremendous rate while the global demand for feldspars remains strong, forcing manufacturers to look for new rock ores rich in feldspars and relatively poor in quartz and ferromagnesian minerals such as syenites.

In Cameroon, several feldspathic rocks were tested for ceramic purpose [20] [25] [26] [27]. Although having concluded that these rocks could be used as feldspar ore for industrial uses, these studies were limited to isolated outcrops on quartz-feldspar veins or pegmatites with a limited extension. It therefore appears necessary to find deposits whose characteristics would dictate the prospects for industrial development, such as alkaline syenites. The syenites of Linté (Centre Region-Cameroon) are an important consideration [28]. They are made of two batholiths: a Northern batholith at Ina and a Southern batholith at Linté. Little work has been carried out on these rocks whose enormous potentialities can be exploited although this valorisation, particularly as a source of industrial feld-

spathic fluxes, depends on knowledge of its physicochemical properties.

This study focuses on the Ina batholith in order to assess its potential as a source of feldspars for industrial uses. Petrographic analysis has been done to identify the different facies, geochemical analysis to understand the distribution of major elements and mineralogical analysis to characterize the rock mineralogy. These rocks were classified and the most probable facies for exploitation as a source of feldspars is identified.

2. Geographic and Geological Context

Located approximately 80 km north of Ngambétikar (Centre region Cameroon), the Ina syenites (Figure 1) cover ~ 1000 km^2 and outcrop within the Precambrian syntectonic granites (Weecksteen, 1957). The study area extends for ~ 350 km^2 between latitudes 05˚45'N and 05˚59'N and longitudes 011˚46'E and 011˚59'E located in a transitional equatorial to tropical climate zone, and covered a vast smooth peneplain whose altitudes dominantly range from 500 to 700 m. The monotonous topography is interrupted by some inselbergs (up to 600 m

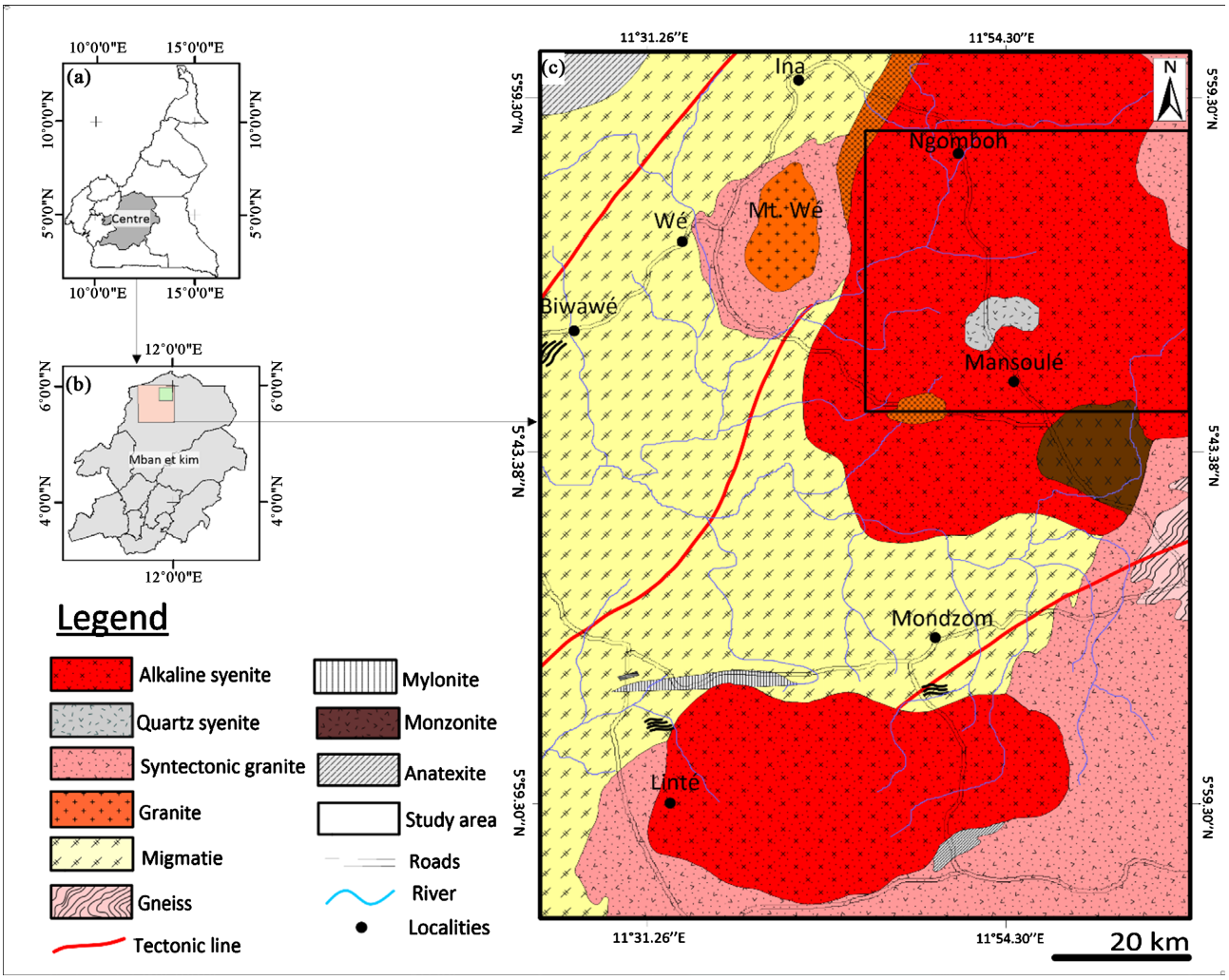

Figure 1. Study area location ((a), (b)) and simplified geological setting (c) modified after [28].

in height) and Mount Wé (2335 m) is the highest hill in the area. We also note an alternation of hills, plains, and lowlands in the sector nestled within the vast depression of the Tikar plain to the south of the Adamawa plateau and the Banyo massifs [29].

The North Equatorial Pan-African Fold Belt is a major collisional belt that holds the region from the West African board to Est African [30] [31]. It is the southernmost branch of the Brazilian Pan-African domain and extends between Cameroon, Tchad, the Central African Republic, the North part of Congo craton and the western Nigeria shield [31] [32]. Among the three different litho-structural domains of the North Equatorial Pan-African Fold Belt defined in Cameroun by [31], the Linté syenite, on which the syenite from Ina batholite depends, belongs to the Centre Cameroon geodynamic domain of the Pan-African North Equatorial Fold Belt. This domain covers a large area stretching from the north of the town of Bafia to the south of the locality of Poli [33]. It is characterized by large rockslides including the Central African Shear Zone [34], the Foumban-Tibati-Banyo Fault [35] [36] and the Sanaga Fault located to the East of Bafia and marked on the 1/500.000 geological of Cameroon, Douala East sheet [28] [37].

The Centre Cameroon domain is marked by several generations of calc-alkaline granitoids with high potassium content, intruded in the high grade gneissic Paleoproterozoic basement [38] [39] [40] [41] [42]. They form a wide variety of rocks like granites, diorites, gabbro and syenites. Depending on the age, the granitoids are syntectonic (630 - 620 Ma), late tectonic (600 - 580 Ma) and post-tectonic (550 Ma) [31] [43]. The plutonic rocks of Linté batholith mainly consist of syenite and monzonite and were emplaced between 590 and 599 Ma, suggesting their classification as syn- to post- collisional granitoids related to the Pan-African Orogeny [44]. Most granitoids are syntectonic belonging to the potassic shoshonitic calc-alkaline series [2]; they are metallic to slightly peraluminous [38] [45] [46] and orthogneissified with a calc-alkaline tendency, high potassic to aluminous [32] [36] [38] [40]. These granitoids have orientations sub-parallel to the Centre Cameroonian Shear Zone.

3. Material and Method

3.1. Field Relationships and Sampling

On the Ina batholith, rock outcrops are widespread and heterogeneous. Identification and description of petrographic types and their sampling have been done based on colour, texture, structure and macroscopic characteristics. Observations were also made on special features such as veins, deposit mode and relationships between the different outcrops. Seventy-five samples were taken from 45 rock outcrops (see sample locations reported on **Figure 2**).

The outcrops of the Ina batholith are abundant and heterogeneous with many blocks, slabs and domes. The colour of the rocks observed on these outcrops varies from whitish (**Figure 3(a)**) to dark grey (**Figure 3(d)**). Numerous erratic, angular or rounded blocks and even monoliths (**Figure 3(a)**) characterize the

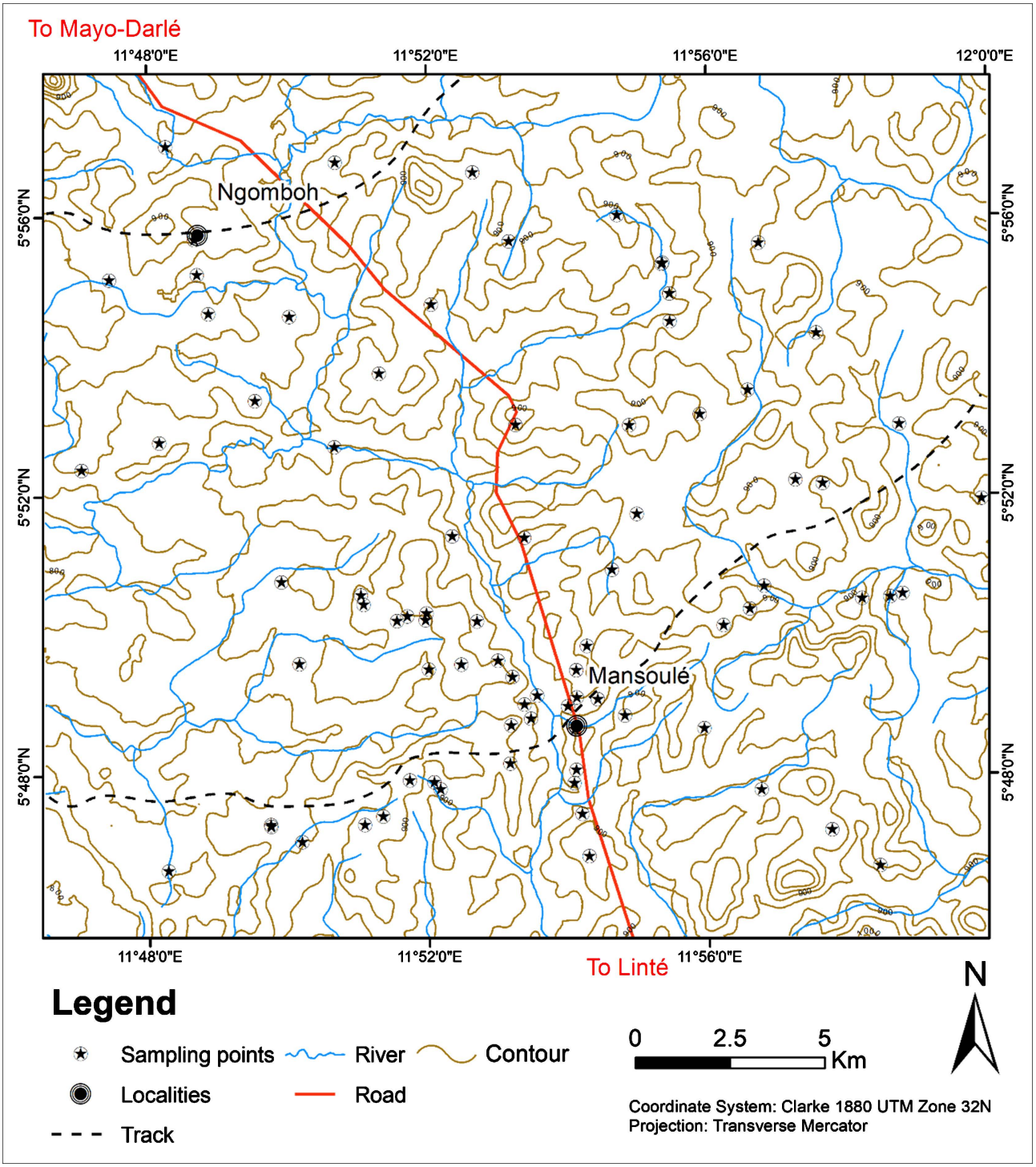

Figure 2. Topographic map of study area with sample locations from modified from Digital Terrain Model (USGS, 2021).

abundant block outcrops. The slab outcrops are large with more or less flattened surfaces (50 to 800 m^2, **Figure 3(b)**), often marked by veins. The outcrops do not present any sign of alteration as is the case with blocks outcrops. The domes outcrops form hills of several meters high (**Figure 3(d)**). The base of these wide domes is boarded by angular blocks detached from the walls of the main hill.

Figure 3. Characteristics outcrops of the Ina batholith. (a) blocs outcrops; (b) slab outcrop; (c) vein on slab and dome outcrop; (d) hill outcrop.

Note that these different types of outcrops are not specifically related to the petrographic types recoded on the Ina batholith syenite and have no structural orientation. Granite, monzonite and granodiorite are sporadically observed as boulders while syenite forms a large slab of ~800 m^2 in the centre of the study area (**Figure 1** and **Figure 4(b)**).

3.2. Petrography

The rock samples were described macroscopically. Textural analyses were performed on thin sections by optical and electron microscope. Forty thin sections were prepared at the Geosciences Department of the University of Padova, Italy. The observations were made using an optical microscope at the University of Liege (Belgium). In order to complete the observations and to determine the semi-quantitative composition of some minerals like magnetite, ilmenite, hematite and perthites, thin sections were observed using a QEMSCAN FEI Quanta 650F electron microscope coupled with energy dispersion spectrometry at RWTH Aachen, Germany.

3.3. X-Ray Diffraction (XRD)

The mineralogical analysis was carried out on more than sixty rocks samples. Mineralogical phases were determined by X-ray diffraction (Bruker D8-Advance Eco 1 kW diffractometer) using monochromatic CuK*a* radiation of 0.020˚ operated at 40 kV and 25 mA using Cu-Ka1 radiation (I = 1.5406 Å) at the laboratory of "*Argiles, Géochimie et Environnements sédimentaires* AGEs", University of Liege (Belgium). Identification of the mineral phases of bulk materials (random

powders < 250 μm in size) was carried out by using EVA software for qualitative estimation and TOPAS software (™ Bruker) software.

3.4. Major and Trace Element Analysis

Major and selected trace elements were analysed using an ARL PERFORM-X 4200 (Rh X-ray tube) X-ray fluorescence spectrometer, Laboratory of Petrology, Geochemistry and Petrophysics of the University of Liège (Belgium). Major element analyses were performed on lithium tetra- and meta-borate fused glass discs prepared with 0.35 g of rock powder. Raw data were corrected following the Traill–Lachance algorithm and calibrated using 66 international standards (basalts, syenites, granites, ultramafic rocks, minerals, and soils). Trace elements (Co, Cu, Ga, Nb, Ni, Rb, Sr, Y, Zn, Zr, Ce, Ba, Cr, and V) were measured on pressed powder pellets. Except for Cr and V, data were corrected for matrix effects by Compton peak monitoring.

Calculations of the Cross, Iddings, Pirson and Washington standards (CIPW) were made on the basis of the major element contents to determine the normative composition.

4. Results and Discussion

4.1. Petrography

The petrographic types of the Ina batholith consist of alkaline syenite, quartz syenite, monzonite, granite and granodiorite. The area is dominated by Neoproterozoic high-K calc-alkaline syenite and monzonite intruding the Paleoproterozoic basement [28].

4.1.1. Syenite

On macroscopic scale, syenites are the most common petrographic type in the study area. The rocks are massive leucocratic to melanocratic with porphyritic texture (**Figure 4(a)**) or phaneritic texture (**Figure 4(b)**). The porphyritic facies are the most abundant, often with a pegmatitic character. These are alkaline syenites made by prismatic phenocrysts of potassium feldspars with malgachite facies (**Figure 4(d)**). These feldspars are grey to dark-grey in colour (**Figure 4(b)** and **Figure 4(d)**), often pinkish (**Figure 4(a)** and **Figure 4(c)**), and show bright and shimmering faces with the Carlsbad twining (**Figure 4(a)**). These sub-automorphic feldspar crystals are joined by an interstitial microlithic ferromagnesian matrix. By shallow alteration, the feldspars remain in relief and the rock shows a rough characteristic surface. Ferromagnesian minerals are dominated by millimetric lamella of biotite. The feldspars from the porphyritic facies are disseminated in a finely crystallized background with biotite and some quartz (**Figure 4(b)**).

Microscopic observations reveal two syenite facies: alkaline syenite and quartz syenite. The alkaline syenite has a porphyritic texture with a pegmatitic character. It almost exclusively shows large phenocrysts of alkali feldspar with plagioclase in some samples. These phenocrysts are linked to each other by a ferromagnesian

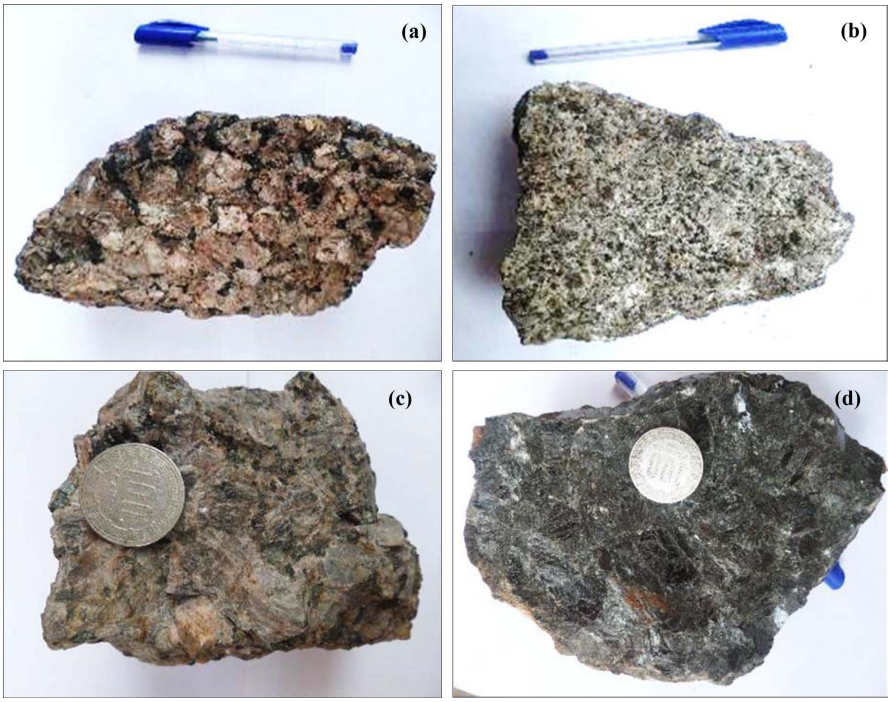

Figure 4. Macroscopic photograph of porphyritic alkaline syenite (a) and quartz syenite (b) identified on the Ina batholith with pinkish feldspars phenocryst (c) and dark-grey feldspars phenocryst with malgachite facies.

matrix consisting of biotite, amphibole and pyroxene entangled and moulded along the crystals of the feldspars or in inclusion. The accessory phases constitute of apatite, titanite and some zircon. In quartz syenite, the rock is grainy in texture and exhibits the same mineralogical characteristics as alkaline syenite except for quartz and higher mesostasis.

Orthoclase is the most abundant alkali feldspar in the rock (80% to 90% modal). It occurs as large (3 to 5 cm), clear automorphic to sub-automorphic with well-marked cleavages, exhibiting the Carlsbad twin (**Figure 5(a)**). Only a few spots show, in polarized light, the distinctive grid pattern of microcline. These feldspars phenocrysts are marked by numerous inclusions of opaque minerals characteristic of the malgachitic type-facies illustrated by the whitish spots in **Figure 5(c)** and **Figure 5(d)**. They are numerous occurrences of perthitic micro textures with exsolutions of sodium feldspars in the form of sparks. These sodium feldspars are close to the albite identified by ESEM-EDX (**Figure 5(d)**). On the one hand, a marginal substitution is observed, followed by a chessboard substitution where albite forming pericline twinning are oriented in both direction of alkali feldspar (**Figure 5(c)**).

Plagioclases are rare (10% to 20% modal) with automorphic to sub-automorphic crystals. They are in the form of large areas with a oscillatory concentric zonation (**Figure 5(b)**) or in the form of elongated rods and marked by a polysynthetic twin of different composition and optical orientation. These plagioclases may contain inclusions of ferromagnesian and opaque minerals (**Figure 5(b)**).

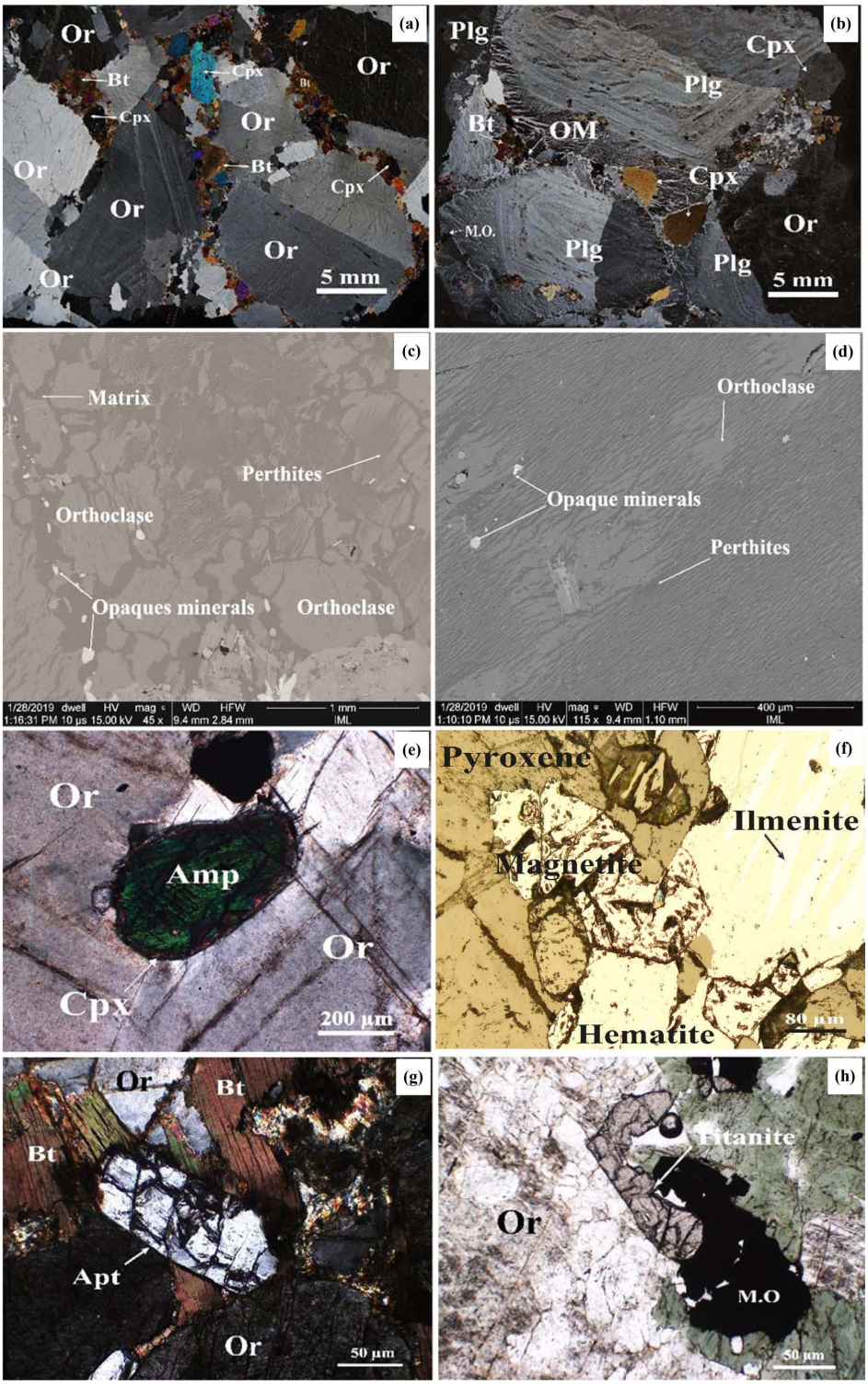

Figure 5. Micro-photographs of Ina syenites. (a) Orthoclase phenocrysts with Carlsbad twin; (b) plagioclase phenocryst with zoned twin; (c) microscopic ferromagnesian in alkali feldspars phenocryst observed by ESEM-EDX; (d) perthites in alkali feldspars phenocryst observed by ESEM-EDX; (e) ouralitization in feldspar phenocryst; (f) magnetite and hematite observed by reflected light in the matrix of feldspars phenocryst; (j) apatite crystal and (k) titanite crystal in the matrix of feldspars phenocrysts. Or: orthoclase, Plg: plagioclase, Bt: Biotite, Cpx: Clinopyroxene, Amp: Amphibole, OM: Opaque minerals, Apt: Apatite.

The cloudy aspect of some plagioclases and potassium feldspars indicates some alteration.

Mica is mainly biotite (<7% modal). It is interstitial and appears as small and sometimes distorted flakes. Some greenish brown flakes underline the transformation of biotite into chlorite during weathering (**Figure 5(a)**). They line up along the edges of the large feldspar crystals with the other ferromagnesian minerals. Pyroxenes (~5% modal) are mainly clinopyroxenes with the characteristic twins of augite. Rare orthopyroxene (*i.e.*, hypersthene) surrounds amphibole (**Figure 5(e)** and **Figure 5(g)**). The amphiboles (green hornblende) are xenomorphic and interstitial in the rock, generally associated with biotite and pyroxenes.

Rounded, sub-angular or angular grains of various sizes and shapes of opaque minerals are scattered in the rock, often in inclusions in other minerals such as K-feldspars. These minerals are identified on reflected light as hematite, ilmenite, hemo-ilmenite (**Figure 5(f)**) and magnetite (**Figure 5(f)**). They represent < 2% modal of the total rock volume.

The accessory minerals are mainly represented by apatite and titanite. Apatite appears as small elongated prisms embedded in other minerals (**Figure 5(g)**). Titanite (**Figure 5(h)**) is observed in small crystals with irregular sub-automorphic contours. Its inclusion in biotite indicates a primary biotite like that of the Monguélé syenites in Southern Cameroon [47].

Quartz is abundant in the grainy facies of syenites (7% modal). It occurs as small ≤ 1 mm sub-automorphic crystals, in interstitial position and seems to be crumpled between the large crystals of feldspars giving it an appearance of a filament (**Figure 5(a)**). Most often, it presents a wavy extinction and is associated with pyroxenes and amphiboles.

4.1.2. Others Granitoids

1) Granite

Granite samples correspond to leucocratic alkaline granites with a porphyritic texture. They contain pink alkali feldspars in phenocrysts and grains of plagioclase feldspars often mixed with quartz (**Figure 6(a)**). The significant presence of slightly oriented biotite flakes between feldspars phenocryst makes these rocks biotite granites (**Figure 6(b)**). Quartz is present as small grains disseminated in a mesostasis formed by ferromagnesian minerals and plagioclases.

At a microscopic scale, the rock is massive, leucocratic with grainy texture. It mainly consists of quartz (~30%) and orthoclase associated with plagioclase, biotite and pyroxene. Quartz is observed as sub-automorphic crystals of millimetre size. Most microcrystal are subcircular with rolling extinction. Some quartz microcrystal is also present as inclusions in feldspar phenocryst.

Orthoclase (**Figure 7(a)**) occurs as millimetric to centimetric crystals with automorphic to sub-automorphic borders. The weathering gives a cloudy appearance to the feldspars. This cloudy appearance represents an association of potassium feldspars and sodium feldspars leading to a perthitic microtexture. Plagioclase is observed in elongated sub-automorphic rods of millimetre to centimetre

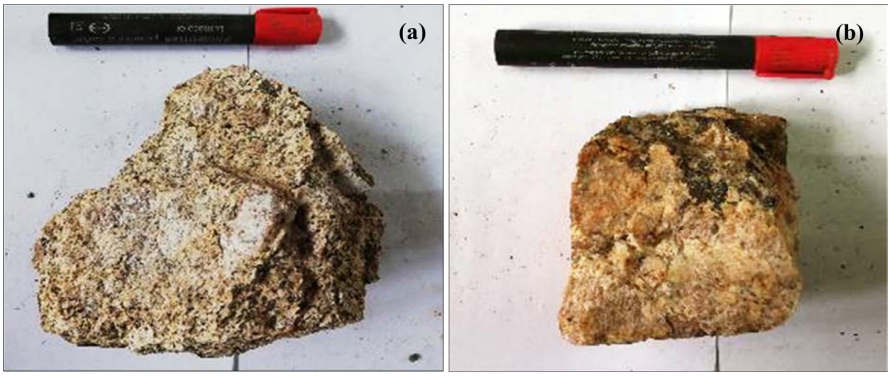

Figure 6. Macroscopic photograph of granite with phaneritic (a) and porphyritic texture (b) samples identified on the Ina batholith.

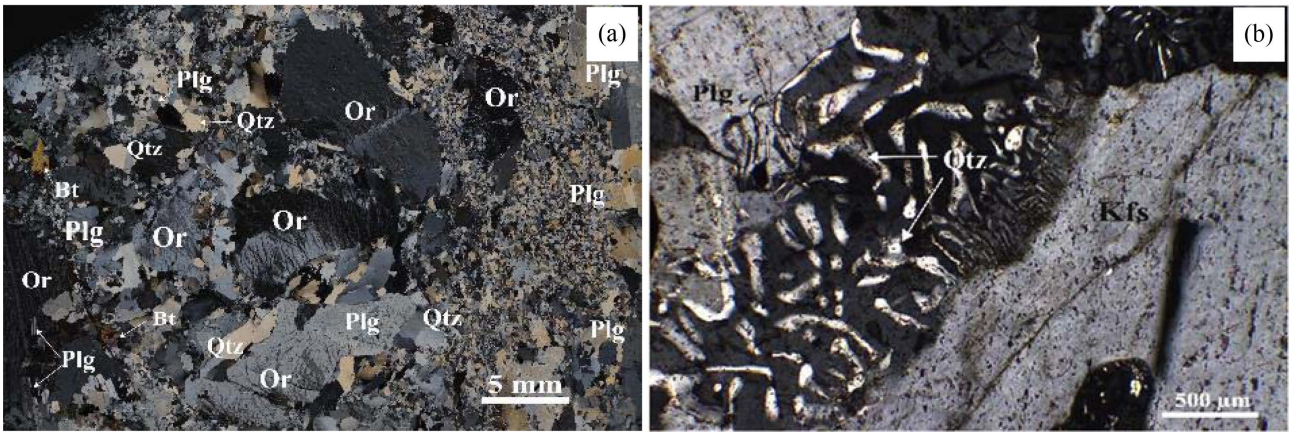

Figure 7. Micro-photographs of alkaline granite; with perthitic feldspars and sub-automorphic quartz (a) and myrmekite microstructure (b) observed in the granite samples of the Ina batholith.

size with common polysynthetic twins. The presence of quartz intergrowths in the alkali feldspars leads to an observed myrmekite microtexture (**Figure 7(b)**).

Biotite occurs as lightly coloured flakes in light to dark brown. These flakes are deformed, frayed and eventually chloritized or even associated with titanite. Pyroxenes are rare (<1% of rock volume), occurring as sub-automorphic augite, interstitial and generally associated with biotite. Opaque minerals (<1% of rock volume) occur in grains of varying sizes in association with ferromagnesian minerals. Accessory minerals are represented by rare titanite observed in the interstices and in association with biotite.

2) Monzonite

Both monzonite and quartz monzonite are found at the site of Ina batholith. The rocks are massive, leucocratic to melanocratic with quartz and without quartz respectively. They have a granular structure where the size of the feldspar crystals varies from millimetric to centimetric. Small crystals of ferromagnesian minerals (biotite, pyroxene, amphibole, and opaque mineral) are more abundant in the quartz monzonite facies (**Figure 8(a)**)

The most abundant minerals in thin section are large feldspars notably ortho-

clase characterized by wide zones (about 2 cm) all marked by the Carlsbad twinning. Plagioclases stand out for their polysynthetic twins. They are elongated rods about the size of the orthoclase (Figure 8(b)). The feldspars in monzonite are characterized by a pinkish colour like in granite. The plagioclases and K-feldspars have a modal composition of ~70%.

Quartz is quite abundant in quartz monzonite but its content varies between the outcrops. They are wavy extinction, automorphic to sub-automorphic crystals. The relative concentration is less than 15%. Biotite is also marked by the presence of flakes which, like in other rocks, are gradually transformed into chlorite. Biotite is also observed in clusters of minerals whose relative abundance is about 10%. Among the other ferromagnesian minerals, we note the presence of amphiboles (*i.e.* green hornblende) and clinopyroxene (e.g. augite). Opaque minerals are present in inclusion in alkali feldspar or plagioclase. A myrmekitic microtexture is also observed.

3) Granodiorite

Granodiorites are massive, brown in colour with an aphanitic structure. These rocks present large centimetric phenocrysts (up to 5 cm) of potassic feldspars sporadically dispersed in a finely grainy matrix (Figure 9(a)) with fine flakes of biotite and small translucent quartz crystals.

On the thin section, the granodiorite is marked by the presence of large centimetric phenocrysts of feldspars dispersed in the finely grained matrix (Figure 9(b)) with fine biotite flakes and small quartz crystals. Feldspars crystals present a malgachitic facies, also visible at a macroscopic scale as syenite.

Granodiorite is made up of alkaline feldspar and plagioclases with quartz, biotite and amphibole as secondary minerals. Opaque minerals constitute the accessory phases. Orthoclase is sub-automorphic and is observed either in large crystals up to 5 cm, or in the form of finely grained crystals all devoid of perthite. The phenocrysts present the Carlsbad twin. Plagioclases appear as small, xenomorphic, whitish crystals abundant in the rock. The polysynthetic twin scratching is rare in crystals. Orthoclase and plagioclase contain inclusions of opaque

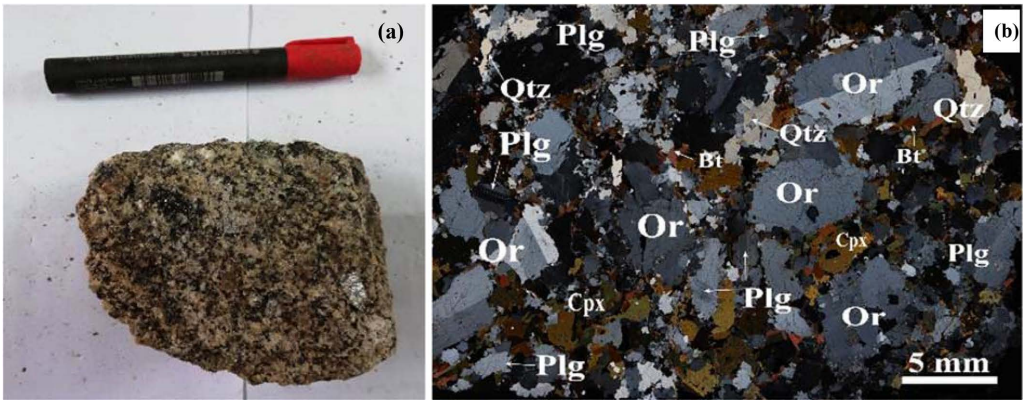

Figure 8. Macroscopic photograph of quartz monzonite sample (a) of Ina batholith and his micro-photographs showing alkali feldspars and plagioclase phenocryst with sub-automorphic quartz and ferromagnesian minerals (biotite, pyroxene and opaque minerals).

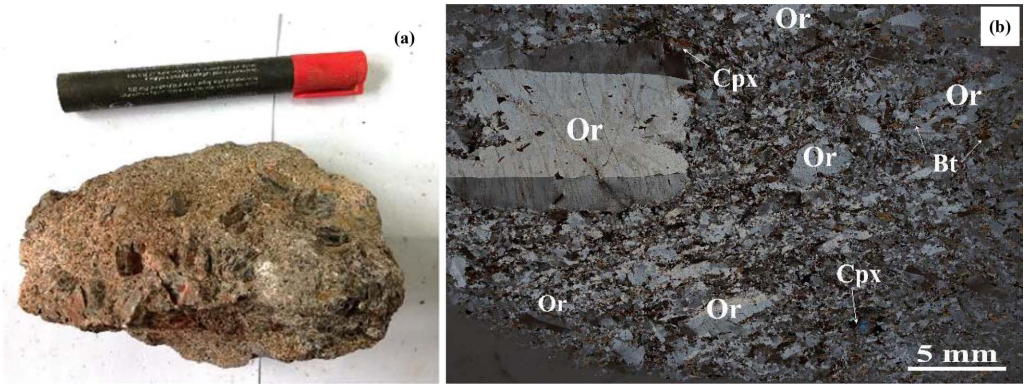

Figure 9. Macroscopic photograph of granodiorite sample (a) of Ina batholith and his micro-photographs showing alkali feldspars phenocryst with ferromagnesian minerals (biotite, pyroxene and opaque minerals).

minerals. Pale yellow to greenish biotite appears as fine flakes or in clusters wide of crystals of orthoclase and plagioclase. Amphibole is disseminated throughout the rock with a relatively high abundance compared to biotite. They are observed in small crystals of olive-green colour and seem to stretch in the length. Rare opaque minerals (magnetite) are included in feldspars.

4.2. Quantitative Mineralogy

Diffractograms and indexing of characteristic hkl lines allowed the identification of the mineral phases and their proportions in each. The indexing diffractograms were selected and grouped according to facies (**Figure 10**). The mineralogical composition of the syenite samples is similar (**Figure 10(a)**) with orthoclase, microcline, albite, anorthite, biotite, augite, green hornblende and some quartz. Except the presence of muscovite in granite and monzonite, the other rock samples of Ina batholith reveal the same mineralogical phases as those identified in the syenites (**Figure 10(b)**) but with different proportions.

The average quantitative estimation of the different mineralogical phases is given in **Table 1**. It is noted that the amount of plagioclase (albite and andesine) is about ~40%. This abundance of plagioclase underlines the presence of cryptoperthites invisible under an optical microscope but detectable by XRD [48].

4.3. Geochemistry

4.3.1. Classification and Nomenclature

The typology of the plutonic rocks suited is based on the classification of [49] which compares the wt% composition of $Na_2O + K_2O$ (total alkali) and SiO_2 oxides. The major element composition of the rocks samples of Ina batholith is consistent with syenite, monzonite, quartz monzonite, granite, granodiorite and monzodiorite (**Figure 11**). However most of the samples plot in the field of alkaline syenites with a high modal content in orthoclase (~85 wt%).

4.3.2. Major elements

The abundance in major and trace elements and the calculated CIPW (*i.e.*,

Cross, Iddings, Persson and Washington) standard for each rock type is presented in Table 2. The major element data of Ina batholith rocks samples shows

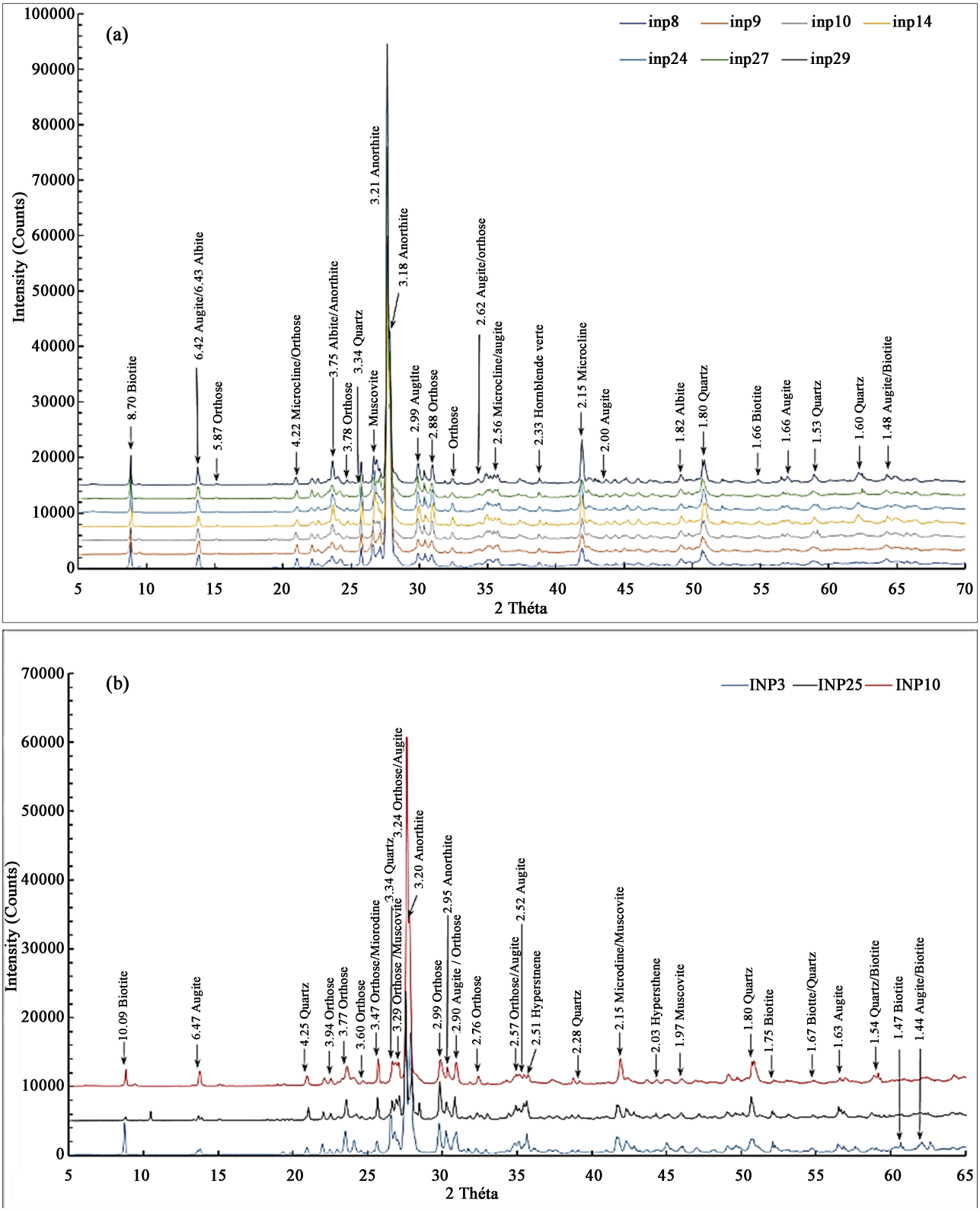

Figure 10. XRD pattern of alkaline syenite samples (A) and some granitoids samples (B) of Ina batholith.

Table 1. Quantitative estimation of the mineralogical phases in the Ina alkaline syenite (a) and Monzonite (b) derived from Topas software (™ Bruker). The abundance is calculated on an average of 25 samples for (a) and 15 for (b).

(a)	Average phase	Weight %
1	Orthoclase	43.43 ± 5.2
2	Albite	24.45 ± 4.7
3	Anorthite	16.39 ± 5.1
4	Augite	9.87 ± 3.7
5	Green hornblende	1.38 ± 2.1
6	Biotite	3.24 ± 2.0
7	Quartz	1.18 ± 1.5
Total	**100.1**	

(b)	Average phase	Weight %
1	Orthoclase	40.80 ±5.3
2	Albite	22.79 ±1.5
3	Anorthite	15.79 ± 1.7
4	Green hornblende	1.54 ± 0.6
5	Augite	9.17 ± 1.8
6	Biotite	2.92 ± 0.3
7	Muscovite	0.14 ± 0.0
7	Quartz	1.10 ± 0.1
Total	**96.0**	

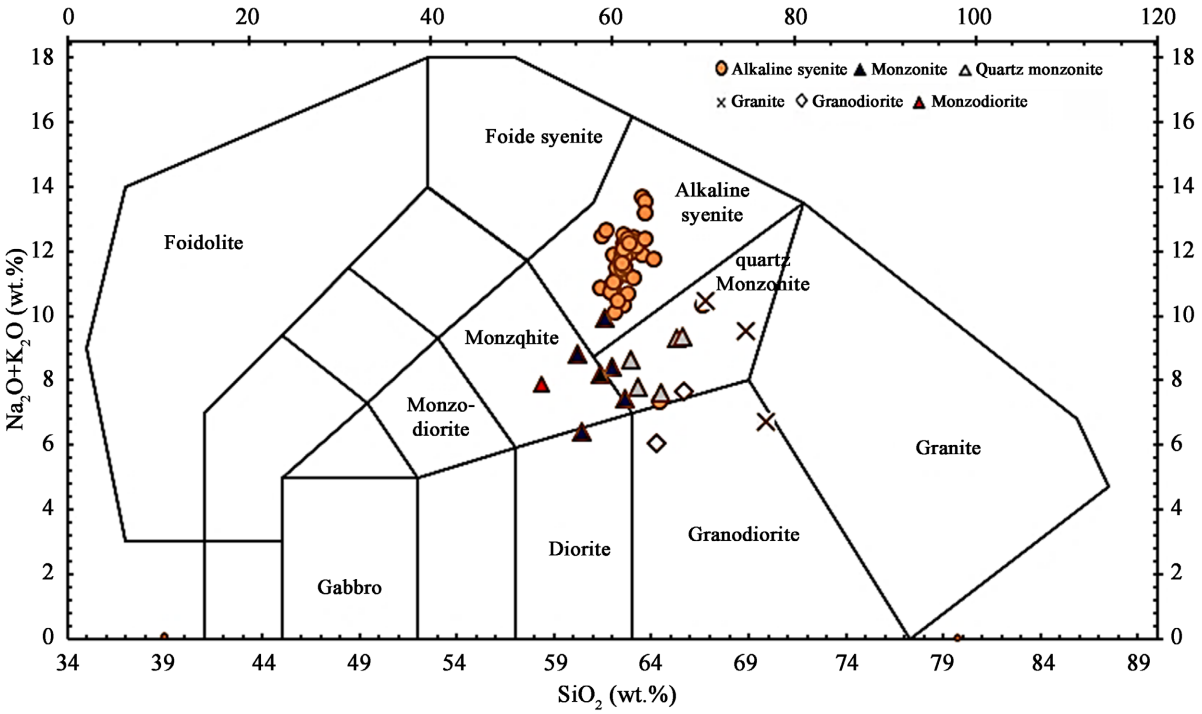

Figure 11. Igneous rocks classification of Ina batholith samples rocks plotted in total Alkali Silica (SiO_2 versus Na_2O + K_2O) diagram according to [49].

a compositional range between 58.68 wt% and 63.63 wt% silica from intermediate rocks (syenite) and up to 77.02 wt% for saturated rocks (granite). The Al_2O_3 content range from 13.91 wt% to 19.81 wt% while the percentage of alkaline oxides ($Na_2O + K_2O$) range from 6.05 wt% to 13.69 wt% with the highest percentage in the intermediate rocks. The content of the other oxides is variable: 0.95 wt% to 8.09 wt% Fe_2O_3, 0.32 wt% to 1.45 wt% TiO_2, 0.35 wt% to 3.52 wt% CaO, (0.13 wt% to 3.98 wt% MgO. The contents in MnO and P_2O_5 are low (<0.8 wt%, **Table 2**).

[50] defined a geochemical boundary in the TAS diagram used to differentiate plutonic suites where all syenite project within the limits of alkaline series (**Figure 12(a)** and **Figure 12(b)**). In the same diagram, some monzonite and granites project into the sub-alkaline series. Frost *et al.*, (2001) [51] proposed a new classification considering the CaO content of samples and allows to define 4 domains between alkaline and calcic series (**Figure 12(c)**). This previous diagram shows that the majority of samples from Ina batholith project into the alkaline suite domain with some samples in the alkaline-calcic and calcic range. It should be noted that all syenite are plotted in the calc-alkaline series. Despite these small variations, the Ina batholith samples are characterized by a marked alkaline composition.

The relative abundance of silica, alumina and alkaline oxides [($SiO_2 > Al_2O_3 > (Na_2O + K_2O)$] and the ratio Al/(Na+K) > 1 indicate a peraluminous composition [52] [53] of most studied rocks (**Figure 12(d)** and **Figure 12(e)**). This peraluminous classification is also justified by the characteristic mineralogy of the Ina batholith rocks samples with the remarkable presence of biotite but also apatite and ilmenite as accessory mineral [52] [54] [55]. However, the K_2O/Na_2O ratio ranging from 1.69 wt% to 3.39 wt% underlines hyperpotassic composition, in agreement with the distribution in the ternary diagram of Marshall (**Figure 12(e)**).

When it comes to major element versus SiO_2, the analysis of the evolution of the major elements refers to the silica saturation diagrams of [56] the Ina batholith rocks samples follow similar differentiation trends. Although the intermediate rocks, notably syenite shows more similarity. The evolution of Na_2O and Al_2O_3 according to the silica content in syenite show positive correlations as Na_2O and Al_2O_3 content increase when the silica decrease (**Figure 13(a)**, **Figure 13(c)**). In the others granitoids, the plotted points are scattered and result in a less distinctive correlation. The evolution of CaO, TiO_2, MgO, Fe_2O_3 and P_2O_5 reflects a similar negative trend (negative correlation) as shown in the **Figure 13(d)**, **Figure 13(e)**, **Figure 13(g)**, **Figure 13(i)**, The absence of strong iron enrichment in rocks as in this case ($0.89 \leq Fe_2O_3$ wt% < 4.69)., indicates an alkaline series in magmatic differentiation [50].

There is a very weak correlation between K_2O and SiO_2 in the syenite and no correlation in the other granitoids rocks (**Figure 13(b)**). Instead, the latter allows for an abundant concentration of K_2O in the silica content range of intermediate

Table 2. Chemical composition of the different rock samples of Ina batholith measured by XRF on bulk rock powder (wt%).

Samples	SiO_2	TiO_2	Al_2O_3	Fe_2O_3	MnO	MgO	CaO	Na_2O	K_2O	P_2O_5	LOI	Total
						Syenite						
INP1	60.10	0.80	16.51	3.50	0.05	2.60	2.57	3.75	7.52	0.37	0.63	98.40
INP2	60.93	0.63	17.40	2.74	0.04	1.92	1.90	3.68	8.36	0.24	0.60	98.44
INP5	61.20	0.64	17.37	2.58	0.05	1.78	1.95	4.04	7.91	0.28	0.51	98.31
INP6	64.68	0.04	19.87	0.76	0.00	0.00	0.11	1.82	10.00	0.03	2.68	99.01
INP8	62.55	0.65	17.50	2.96	0.06	2.20	2.05	3.80	8.38	0.32	0.48	99.02
INP9	59.40	0.62	16.27	3.96	0.06	3.72	2.97	3.09	7.77	0.45	0.82	99.14
INP10	59.88	0.66	16.90	3.30	0.06	2.46	2.35	3.38	8.08	0.36	0.75	98.18
INP12	62.22	0.56	17.70	2.29	0.03	1.68	1.69	3.65	8.43	0.23	0.81	99.30
INP13	62.11	0.66	17.73	2.90	0.04	2.04	2.22	3.41	8.69	0.35	0.59	97.65
INP14	60.06	0.63	17.29	2.75	0.04	2.06	2.01	3.40	8.50	0.30	0.60	99.92
INP141	61.36	0.65	17.53	2.91	0.04	2.18	2.13	3.44	8.66	0.35	0.67	99.92
INP15	60.10	0.71	16.48	4.21	0.07	3.98	3.15	2.97	7.85	0.47	0.01	99.09
INP17	60.54	0.68	17.08	3.20	0.07	2.48	2.21	3.66	7.72	0.33	0.69	98.66
INP19	59.51	0.61	16.74	4.16	0.08	3.56	3.26	3.56	6.42	0.47	0.40	98.76
INP21	61.51	0.73	16.21	4.33	0.08	3.52	3.25	3.78	6.61	0.46	0.51	99.79
INP23	59.02	0.68	16.58	3.30	0.05	2.59	2.02	3.44	8.14	0.34	0.60	96.77
INP231	61.25	0.70	17.17	3.37	0.05	2.67	2.06	3.49	8.27	0.35	0.65	100.04
INP24	59.88	0.64	17.03	3.18	0.06	2.45	2.19	3.43	7.99	0.30	1.15	98.30
INP26	61.35	0.59	17.52	2.94	0.05	2.36	2.22	3.35	8.48	0.32	0.81	99.98
INP27	60.93	0.66	17.14	3.35	0.05	2.65	2.54	3.32	8.40	0.38	0.65	100.08
INP281	59.00	0.64	17.50	2.55	0.04	1.77	1.90	3.28	8.78	0.26	0.67	96.38
INP282	60.80	0.76	17.45	2.85	0.05	2.10	2.07	3.18	8.83	0.31	0.91	99.32
INP283	61.35	0.66	18.04	2.60	0.04	1.82	1.97	3.35	8.99	0.28	0.43	99.53
INP29	60.79	0.57	17.19	3.25	0.05	2.51	2.39	3.34	8.25	0.35	0.84	99.55
INP30	61.67	0.62	17.43	2.67	0.04	1.88	2.02	3.67	8.54	0.30	0.80	99.64
INP31	60.07	0.62	16.85	3.98	0.06	3.32	2.86	3.23	7.85	0.45	0.72	100.02
INP33	61.36	0.62	17.70	2.68	0.04	1.81	1.89	3.52	8.61	0.29	1.08	99.59
INP34	59.95	0.69	17.42	2.91	0.05	2.05	2.22	3.29	8.48	0.32	0.63	98.00
INP35	61.37	0.67	17.75	2.87	0.05	1.99	1.81	3.48	8.51	0.30	0.46	99.25
INP371	60.52	0.53	17.69	2.37	0.03	1.52	1.76	3.54	8.49	0.25	0.50	97.21
INP372	58.94	0.31	18.43	0.89	0.02	0.12	0.34	3.45	9.29	0.07	1.28	93.14
INP373	62.02	0.55	18.04	2.42	0.03	1.55	1.79	3.67	8.70	0.26	0.46	99.48
INP374	63.56	0.32	19.78	0.91	0.02	0.17	0.35	3.67	9.86	0.07	1.18	99.89

Continued

INP39	63.35	0.63	18.52	2.45	0.04	1.60	1.55	3.65	8.82	0.27	0.56	101.44
INP41	60.66	0.74	17.90	2.95	0.06	1.91	1.74	3.62	8.53	0.33	0.77	99.22
INP44	59.02	0.64	16.17	3.61	0.06	3.16	2.80	3.29	7.59	0.39	0.95	97.68
INP47	57.55	1.42	17.52	4.46	0.04	1.83	1.47	2.78	9.43	0.60	0.64	97.74
INP48	59.46	1.57	17.41	4.69	0.04	1.83	1.66	2.92	9.78	0.63	0.29	100.29
INP51	60.56	1.00	16.97	3.72	0.05	1.65	1.66	4.12	7.94	0.33	0.39	98.39
INP52	63.85	0.51	18.47	2.11	0.03	0.69	0.74	4.44	8.82	0.23	0.55	100.42
INP54	59.92	0.65	16.65	3.95	0.06	3.11	2.69	3.21	8.16	0.45	0.25	99.10
INA1	60.54	1.04	15.51	4.66	0.07	2.45	2.49	3.89	6.59	0.38	0.44	98.06
INA2	59.95	0.52	16.76	3.07	0.04	2.43	2.45	2.87	8.10	0.38	0.58	97.16
INAG1	62.06	0.91	17.35	2.75	0.03	1.15	1.34	3.94	7.74	0.24	0.57	98.10
INAG2	61.31	1.31	17.58	3.97	0.04	1.18	1.12	4.08	7.83	0.33	-0.60	98.15
INAG3	60.48	0.77	17.13	3.18	0.05	1.98	1.98	3.78	7.09	0.29	0.41	97.15
Average	60.84	0.69	17.37	3.07	0.05	2.10	2.00	3.47	8.30	0.33	0.68	98.75
						Monzonite						
INP3	57.77	0.45	13.83	6.02	0.11	6.76	4.26	2.99	5.05	0.60	0.58	98.42
INP22	58.06	0.33	15.51	4.34	0.08	4.24	3.84	2.36	7.34	0.78	1.20	98.07
INP25	55.20	1.17	14.40	8.75	0.17	3.37	5.60	2.25	6.38	0.52	0.33	98.15
INP441	51.44	0.54	14.07	3.06	0.05	2.55	2.40	3.19	6.40	0.35	0.98	85.03
INP43	67.15	0.38	17.07	2.40	0.05	0.83	2.10	3.80	5.52	0.16	0.43	99.89
INP45	62.45	0.83	16.86	4.97	0.09	1.95	3.68	4.27	3.45	0.36	0.52	99.44
INP55	67.52	0.25	15.38	1.46	0.02	0.36	0.38	3.04	6.95	0.16	0.95	96.46
INA4	60.29	0.63	17.80	4.36	0.08	1.73	3.12	3.72	4.66	0.28	0.55	97.23
INA6	63.81	0.84	15.64	4.61	0.08	1.78	2.96	3.19	4.02	0.43	0.47	97.82
INA8	64.61	0.63	16.16	4.18	0.06	1.66	2.99	3.33	4.17	0.27	0.63	98.70
INA10	56.59	0.93	17.05	5.50	0.08	1.85	3.51	2.99	4.95	0.39	0.51	94.35
INA22	57.19	1.08	15.42	5.61	0.07	3.07	3.44	1.94	8.66	0.70	0.44	97.60
						Others granitoids						
INP4	74.33	0.08	14.01	0.54	0.01	0.12	0.30	3.39	6.07	0.03	0.43	99.32
INP53	52.43	1.01	15.64	7.13	0.13	2.82	4.95	3.03	4.87	0.40	8.05	100.46
INP551	70.35	0.25	15.72	1.49	0.01	0.30	0.38	3.21	7.25	0.17	0.81	99.94
INA9	75.99	0.03	13.72	0.42	0.01	0.00	1.58	3.06	3.54	0.03	0.28	98.67
INP46	66.98	0.38	16.15	2.45	0.04	0.82	1.70	3.09	4.45	0.13	2.48	98.67
INA7	63.80	0.72	15.65	5.31	0.10	1.70	3.80	3.90	2.04	0.22	1.02	98.27
INP18	56.07	0.46	11.08	7.99	0.17	9.03	4.54	1.94	4.36	0.94	0.25	98.83

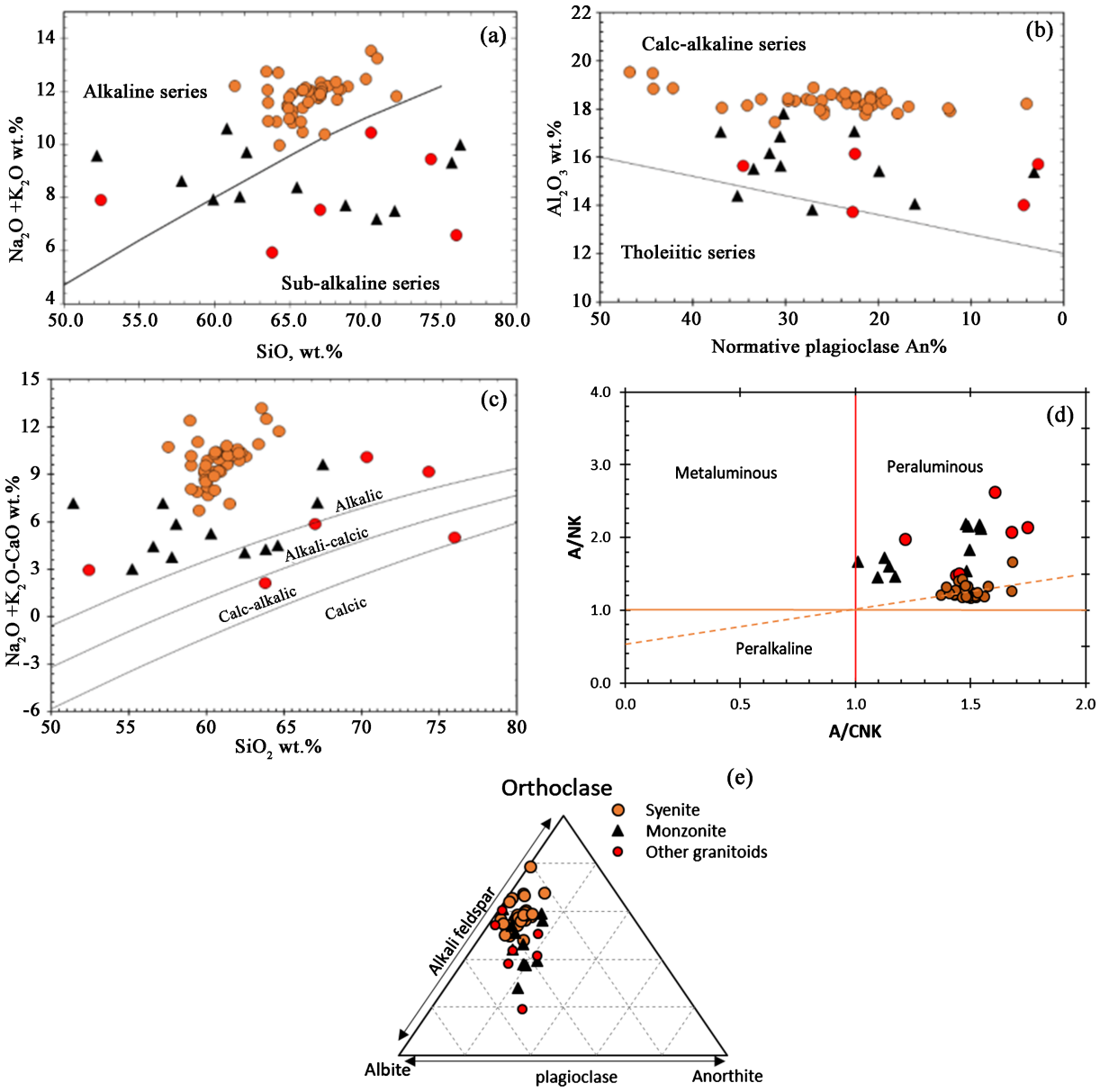

Figure 12. Magmatic classification series of rock samples of the Ina batholith. (a) $Na_2O + K_2O$ vs SiO_2 [50], (b) Al_2O_3 vs normative plagioclase (An wt%) [50], (c) $Na_2O + K_2O$ - CaO wt % vs SiO_2 [51], (d) A/NK vs A/CNK [53], and (e) Albite, anorthite and orthoclase ternary diagram of [57].

rock with very slight variations in their content ($7.52 \leq$ wt% $K_2O < 9.78$). This can be explained by the abundance of alkaline syenite among the studied samples and also by the fact that these syenite are hyperpotassic [57] (**Figure 12(e)**).

The calculation of the CIPW standard allows to identify the theoretical composition of felsic and accessory minerals For Ina syenites, two facies are distinguished by their normative quartz composition: alkaline syenites with low quartz content (At most 4.77 wt%) and quartz syenites with quartz content ≥ 5 wt% The normative orthoclase is abundant, ranging between 38.39 wt% and 57.02 wt%. Plagioclase ranges from 24.42 wt% to 41.35 wt%. Ferromagnesian and accessory minerals are the same as observed in the thin sections. The anorthite

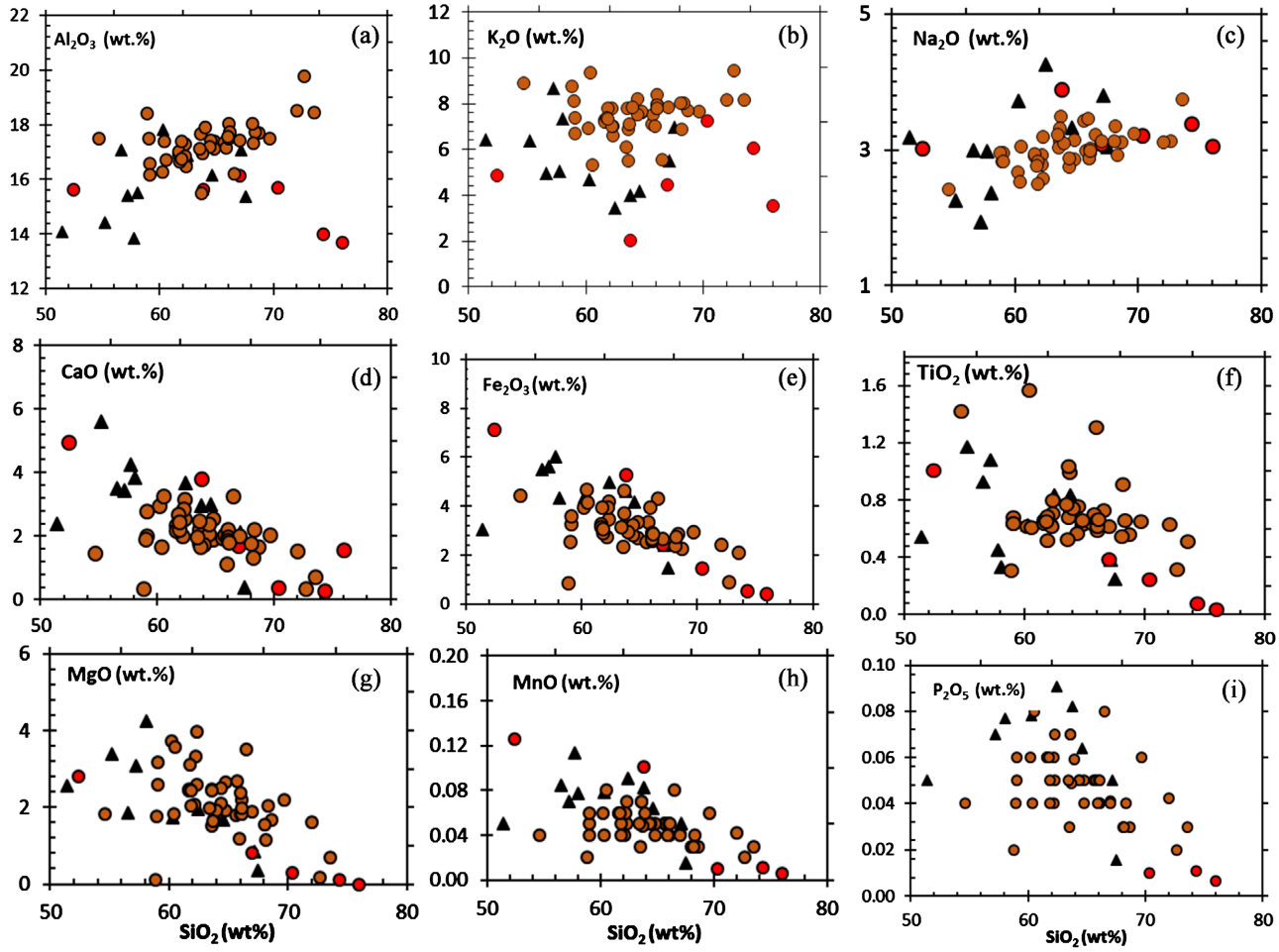

Figure 13. Hacker variation diagram of some major elements (in wt% oxide) versus SiO_2 of the Ina batholith rocks samples [63].

proportion of plagioclases range from An2 to An26.30 proof that plagioclases are sodic and therefore, very close to albite.

4.3.3. Trace Elements

The trace elements data of Ina batholith samples (**Table 3**) indicate high values in Ba which varies from 2159 to 4953 ppm in the syenite and from 2470 to 6664 ppm in the monzonite. In granite and granodiorite, Ba ranges from 892 to 2159 ppm and to 1905 to 2159 ppm, respectively. Sr is also characterized by high abundance from 848 to 1477 ppm in syenite and 356 to 2274 ppm in monzonite. On the contrary, Nb, Pb, Co, Cu, Y and Ga display the lowest values, ranging between 10 and 300 ppm at most.

The parallel evolution of trace and major elements in the Harker diagrams (**Figure 14**) shows similar behaviours with silica enrichment for Ba, Sr, Rb and Zr. In contrast Cr and Ni present a negative correlation with silica in all studied petrography types. The classification diagram of Whalen *et al.* (1987) [58] shows that most petrographic types of the Ina batholith samples belong to the others granites, notably designated by the letters "S" and "I" nomenclature according to [59] and MPG nomenclature of [60]. Recently these nomenclatures (S and I) have

Table 3. Trace element (ppm) of granite, granodiorite and monzodiorite of the Ina batholith. Note nd indicates values not detected by the XRF.

Samples	Co	Cu	Ga	Nb	Ni	Rb	Sr	Y	Zn	Zr	Ba	Ce	Cr	V
							Syenite							
INP1	12	10	16	15	49	247	1307	15	43	329	3770	78	55	66
INP2	10	33	21	18	38	280	1380	10	35	131	4085	46	40	54
INP5	9	29	21	20	36	265	1323	11	36	162	2697	76	8	47
INP6	5	nd	40	15	4	530	65	5	5	88	149	41	6	4
INP8	10	36	20	16	47	290	1328	16	52	127	4371	55	47	54
INP9	14	20	18	13	77	250	1342	18	50	104	4251	68	85	65
INP10	14	18	14	6	68	279	1465	21	57	103	4457	55	60	65
INP12	9	nd	16	8	38	275	1439	23	31	109	4387	46	35	47
INP13	11	45	19	15	51	265	1382	17	43	121	4626	84	44	60
INP14	12	23	20	15	58	273	1453	25	47	113	4805	35	37	53
INP15	16	13	18	13	96	217	1352	67	53	81	4031	39	90	71
INP17	12	29	20	14	59	236	1225	15	44	94	3888	52	55	61
INP19	14	11	19	11	59	136	1208	15	54	60	3337	62	88	67
INP21	13	46	20	15	63	181	1141	20	55	172	3151	80	78	72
INP23	12	32	19	15	56	276	1413	15	42	108	4297	72	55	63
INP24	17	36	20	15	80	272	1356	16	52	102	4314	69	55	57
INP26	12	14	19	12	57	269	1477	15	34	90	4592	28	47	49
INP27	11	17	19	13	58	278	1410	22	46	98	4460	55	51	60
INP281	11	29	20	15	51	285	1464	11	33	113	4953	9	38	53
INP282	11	29	20	15	51	285	1464	11	33	113	nd	nd	nd	nd
INP29	10	42	19	12	53	281	1449	15	43	89	4619	30	41	52
INP30	10	51	19	13	45	274	1357	13	31	87	4689	30	35	51
INP31	14	4	14	5	73	258	1373	15	44	138	4296	45	76	67
INP33	10	13	15	6	35	271	1509	10	31	109	4717	35	36	52
INP34	9	36	21	14	38	282	1462	10	35	113	4665	26	34	52
INP35	12	9	15	9	62	283	1522	12	39	145	4557	12	44	59
INP371	11	32	20	15	39	301	1331	11	34	100	4395	43	36	56
INP372	8	35	21	13	32	281	1400	6	13	109	4526	38	34	51
INP373	5	25	23	15	8	294	1476	15	44	151	nd	nd	nd	nd
INP374	13	27	19	14	67	254	1324	19	50	113	4094	71	73	63
INP39	9	28	20	15	32	305	1396	9	33	107	4684	22	29	48.85
INP41	10	66	21	14	39	346	1336	12	45	112	nd	nd	nd	nd

Continued

INP44	13	27	19	14	67	254	1324	15	44	113	4094	71	73	63
INP47	12	236	23	14	22	364	1057	10	29	66	1379	203	1	127
INP48	7	52	25	12	8	305	848	16	46	75	nd	nd	nd	nd
INP51	12	11	13	5	58	273	1477	16	46	198	3180	90	21	82.01
INP52	12	11	13	5	58	273	1477	nd	nd	198	4622	57	62	68
Monzonite														
INP3	8	nd	18	5	2	133	877	10	50	142	3234	32	7	38
INP22	11	15	23	18	12	71	953	20	102	242	2470	103	16	82
INP25	19	64	16	23	41	158	1342	33	139	316	5811	96	53	131
INP441	10	153	22	14	22	388	1138	17	52	64	1879	194	3	121
INP43	8	nd	18	5	2	133	877	10	50	142	3216	43	8	37
INP45	17	4	12	8	30	78	1504	28	102	305	3753	65	43	121
INP55	6	0	16	12	7	236	694	7	14	191	2159	31	10	21
INA6	23	nd	11	5	192	152	1395	21	84	208	3741	78	212	66
INA8	15	20	15	8	67	137	2274	16	53	34	6664	29	81	nd
Others granitoids														
INP4	5	nd	15	8	nd	202	356	6	4	40	892	38	4	8
INP46	7	nd	22	11	5	76	727	12	49	137	1945	76	8	32
INP18	29	4	12	8	184	113	1051	34	113	84	2836	161	371	86

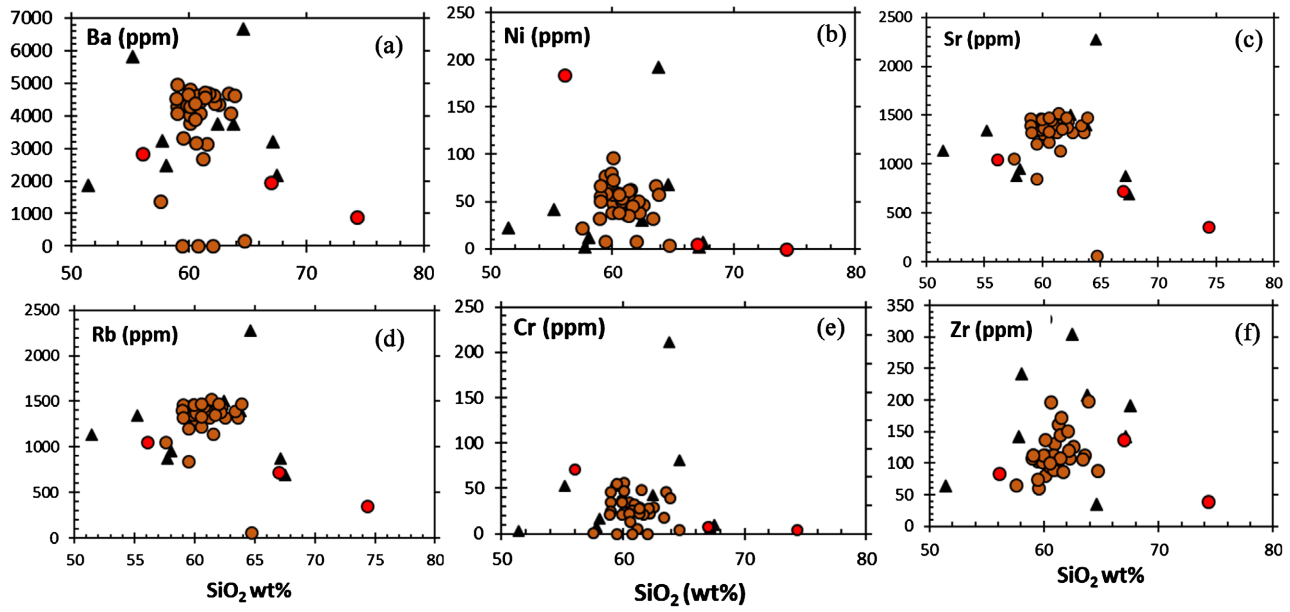

Figure 14. Hacker variation diagram of some trace elements of Ina batholith syenite [63].

been associated to granitoids and not only to the granites [54] (**Figure 15(a)**). The diagram of [61] confirms that most samples belong to the anorogenic domain of syn-collisional granitic magma (**Figure 15(b)**), with Y/Nb values < 1.2

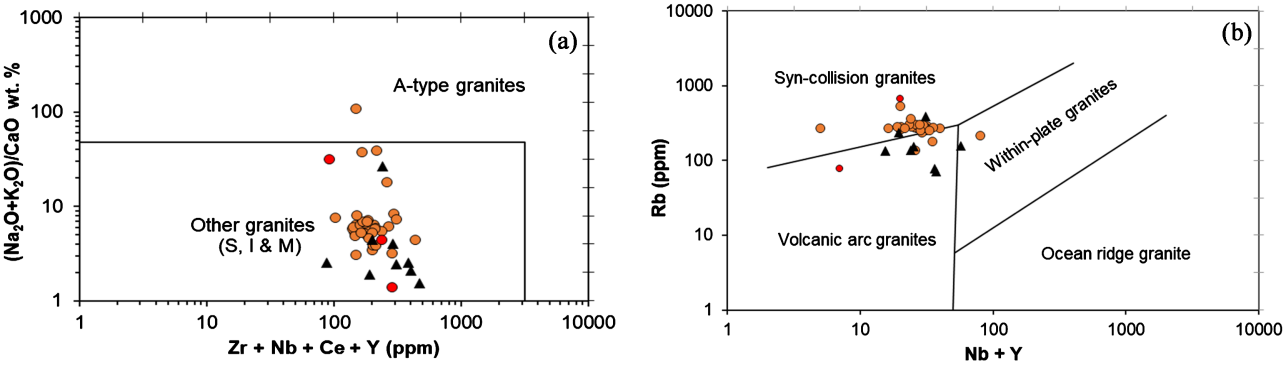

Figure 15. Diagram showing the setting of Ina batholite rocks; (a) diagram from [58] and (b) diagram from [61].

ppm characteristics of most alkaline suites [62].

5. Potential of Ina Syenite as a Source of Feldspathic Flux

In general, several igneous rocks whose petrographic and geochemical classification obeys a certain standard are exploited as alternative telepathic flux raw material for ceramics and glass industries [18]. These include alkaline syenite and quartz syenite [3] [6] [19] [21] [22] [64] [65], monzonite and quartz monzonite [19], granite [17] [19] and even gneiss [66]. The rock samples of Ina batholith, according the geochemical characterization and nomenclature from the TAS diagram [49], belong to the range of these igneous rocks used as feldspathic fluxes.

Syenite, due to their specify, are among the most requested rocks as alternative source for feldspathic flux worldwide [4] [17] [22] [67] [68]. For this purpose, several characteristics criteria based on petrographic features, mineralogical and geochemical composition are analysed. These syenites are the most common petrographic type in the Ina batholith and therefore require special attention others petrographic types (monzonite and granite) that are also potentially valuable but are not enough present on the study site.

Petrographic analysis of rocks samples of Ina shows that they are mainly composed of bulky K-feldspars phenocryst, sometimes plagioclases phenocryst (at least 85 wt% of feldspar) and ferromagnesian minerals such as those in the syenite study by [19] [69]. Although feldspars phenocrysts is the main mineral, its purity is affected by the presence in the form of inclusion of ferromagnesian, accessory minerals but especially ferrous opaque minerals leading to the dark grey color of these feldspars with the so-called malgachite facies [70]. The recurrent observation of perthites in K-feldspars compensates for the low presence of plagioclases, particularly sodium plagioclase and thus the increasing of sodium content of Ina syenite as feldspathic flux raw material [17]. Quartz identified in some petrographic type also plays a key role in ceramic production at it increase stiffness, prevent deformation and reduce capillary cracking and thermal expansion of the product [71]. The fineness of the ferromagnesian matrix of these rocks has an impact on its structural nature which is also essential in that crush-

ing and grinding could be done with reduced energy consumption [72].

On the geochemical level, the contents specially sought in commercial feldspathic flux raw materials are those of alumina, potassium, sodium, iron and titanium. The minimum required alumina content is 16 wt% [73]; yet the Ina syenite have high contents (15 ≥ wt% Al_2O_3 ≥ 20) for an average of 17.03 wt% (**Table 2**). The relation [(SiO_2 > Al_2O_3 > (Na_2O + K_2O)] and the ratio Al/(Ca + Na + K) > 1 which is Alumina Saturation Index (ASI) justifies the peraluminous nature of all Ina batholith syenite samples. This in accordance to Shand diagram (1943) (**Figure 16(a)**) as the most part of the granitoids ores exploited worldwide [19]. This alumina improves the hardness, flexibility and mechanical strength of the ceramic products and chemical resistance of the glass [21] [65] [74].

The minimum content required for total alkali (K_2O + Na_2O) is 6 wt%. They are considered as the main melting oxides whose role is to control fusibility [17] [73]. However, the total alkali content of Ina syenite is very high (10.10 ≥ wt% K_2O + Na_2O ≥ 13.69) and the average is about 11.48 wt%. The **Figure 16(b)** [57] shows the potassic character of the Ina syenite. In addition, the result show

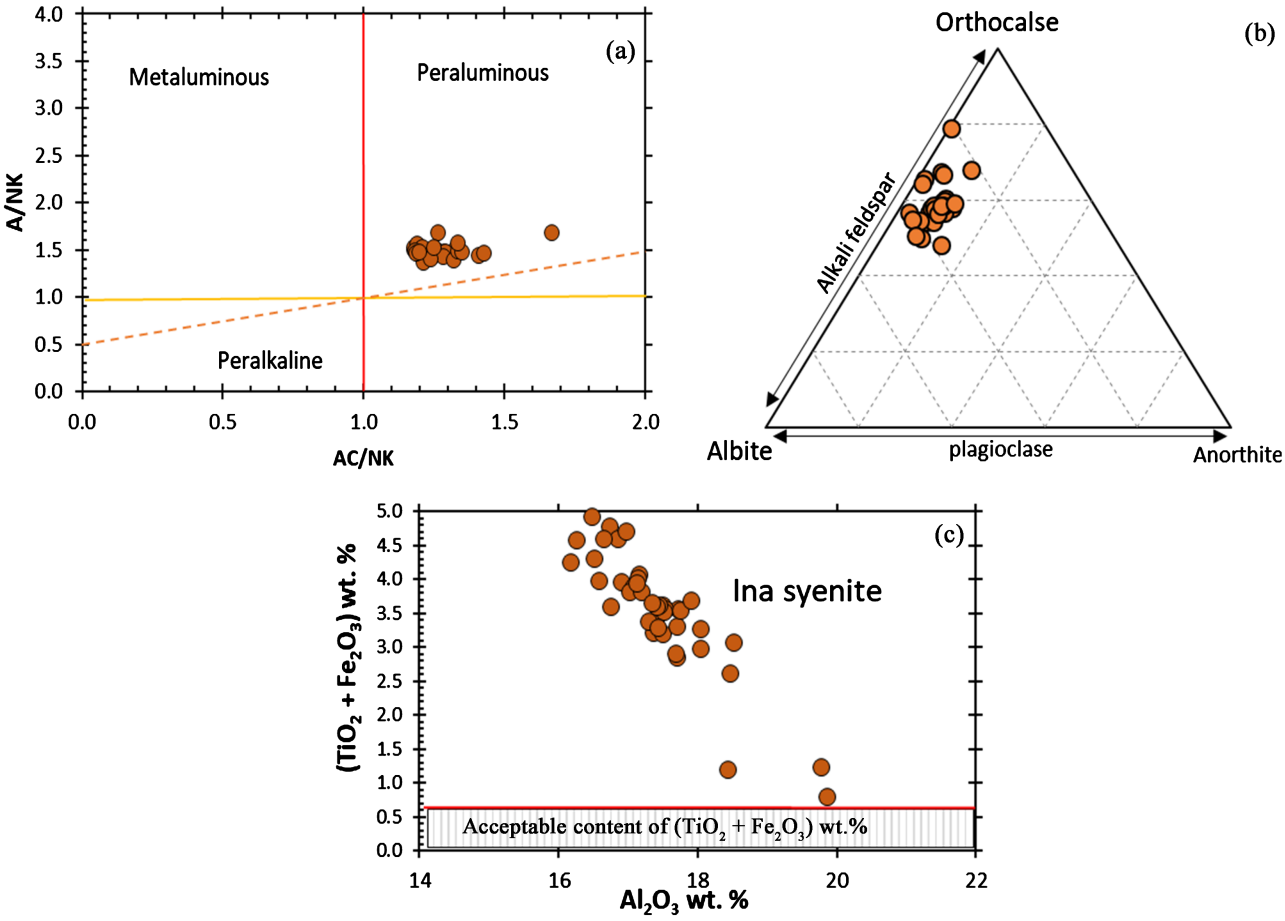

Figure 16. Geochemical classification of Ina syenite according to feldspar ores worldwide, (a) A/CNK vs A/KN Shand diagram (1943) and (b) Orthoclase-Albite-Anorthite ternary diagram of [57] and (c) wt% Fe_2O_3 + wt% TiO_2 content of Ina alkaline syenite compared to [73] norm.

higher total alkali content of Ina syenite compared to the feldspar ore of the world's specialized feldspars ores [Germany (9 wt%), Sweden (8.83 wt%), Norway (9.20 wt%), Czech (7.89 wt%) and Japan (7.58 wt%)] [17].

In the Ina syenite, the iron ($1 \geq$ wt% $Fe_2O_3 \geq 5$) and titanium ($0.4 \geq$ wt% $TiO_2 \geq 1$) content are very high (**Figure 16(c)**) compared to the minimum required which varies from 0.01 to 0.5 depending on their use [73]. this amount of colored element reduces the purity of the feldspars and has a significant impact on its whiteness.

Indeed, according to data of Ina syenite, they can be suitable in ceramic and glass industries like some of other feldspars ores studied around the world (**Figure 17**) despite a high content of iron, titanium and other colored minerals which are considered harmful to ceramics and glass applications. Thus, several scientific works have shown that it's possible to carry out purification and enrichment treatments of feldspar ores that increase the content of alumina and melting elements in the one hand and reduce the impurity contents. These treatments consist of magnetic separation that removes iron bearing and titanium bearing minerals [15] [75] [76] [77] [78]. Magnetic separation is most often followed by flotation adapted for colored minerals [75] [79] [80] [81]. Flotation also allows to isolate K-feldpar from Na-feldspar [82] [83]. The high ppm content of trace elements such as Ba and Sr in the Ina batholith syenite samples has no impact on the potential of these rocks as a feldspathic flux for the ceramic and glass industries.

At the end, ceramics tests are still needed to approve the use as raw material in these industries. The high traces elements content in Ba and Sr of Ina batholith samples has no impact on the potential of these rocks as a feldspathic flux for ceramics and glasses industries but also as a source of potassium for agricultural amendment [9]. In addition, the granite, monzonite and granodiorite of the Ina

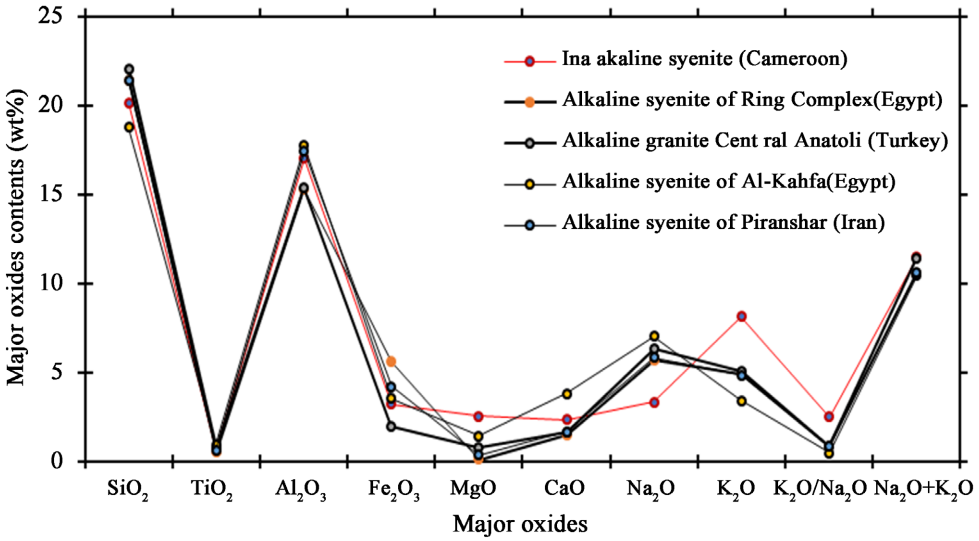

Figure 17. Comparative curves of chemical composition of alkaline syenite of Ina batholith and some other feldspars ores suited around the world with SiO_2 wt%/3.

site can also be used as a source of feldspathic flux. These rocks, including syenite, can be exploited as dimension stones [4] [7] [8].

6. Conclusion

The aim of this study was to characterise the rocks of Ina batholith with a particular focus on syenites in order to assess its industrial mineral potential. Based on petrography, mineralogy and geochemistry, the Ina batholith consists of syenites (alkaline syenite and quartz syenite) and other granitoids including granitic bedrock, monzonite and granodiorite intrusion. Syenite ranging in composition from predominantly alkaline syenite to minority quartz syenite is far the most promising petrographic type. Petrographic examinations of the samples show that the rocks mainly consist of alkali feldspar phenocryst and plagioclases well as minor amounts of various ferromagnesian mineral (chloritized biotite, clinopyroxenes, and amphiboles). These feldspar phenocrysts are characterised by their dark grey hue due to the presence of several opaque minerals' inclusions (ilmenite, hematite, magnetite) and some accessory minerals (titanite). There are also numerous perthites and cryptoperthites established by exsolutions of sodium feldspars. In addition, quartz is observed as interstitial microcrystals or as micrographic intergrowth with alkali feldspar.

Geochemical analysis of the major elements reveals proportions of silica that range from intermediated rocks (58.68 wt%) to saturated rocks (7702 wt%). The results also indicate alumina contents range between 15.08 wt% and 19.80 wt% with an average of 17.03 wt%, total alkali range between 10.30 wt% and 12.30 wt% with an average of 11.48 wt%; K_2O/Na_2O ratio varies between 1.65 wt% and 5.51 wt% with an average of 2.58. In contrast, the iron and titanium contents are quite low (<5 wt%). These geochemical data justified the fact that all syenites are metaluminous and ultrapotassic. These data underline that alkaline syenites of Ina are more suitable for the ceramic and glass industry than some feldspathic fluxes ores of the same category mined throughout the world.

Acknowledgments

The data are part of the doctoral thesis of the first author at the Department of Geology, of the University of Liège (Belgium) in co-diplomation with the Department of Earth Sciences of the University of Yaoundé I, Cameroon. The first author would like to thank ARES-CCD for the PhD grant and technical support.

Conflicts of Interest

The authors declare no conflicts of interest regarding the publication of this paper.

References

[1] Kuang, G., Xu, C., Shi, A., Liu, Z. and Wei, C. (2020) Mineralogical and Geochemical Constraints on Origin of Paleoproterozoic Clinopyroxene Syenite in Trans-North China Orogen. *Precambrian Research*, **337**, Article ID: 105557.

https://doi.org/10.1016/j.precamres.2019.105557

[2] Dawaï, D., Bouchez, J.L., Paquette, J.L. and Tchameni, R. (2013) The Pan-African Quartz-Syenite of Guider (North-Cameroon): Magnetic Fabric and U-Pb Dating of a Late-Orogenic Emplacement. *Precambrian Research*, **236**, 132-144. https://doi.org/10.1016/j.precamres.2013.07.008

[3] Everard, J.L. (1996) An Assessment of the Resource Potential for Nepheline Syenite at Cygnet and Elsewhere in Tasmania. Tasmanian Geological Survey Record 1996/13, 16 p.

[4] Kanouo, N.S., Wang, L., Kouske, A.P., Yomeun, S.B. and Basua, E.A.A. (2019) Petro-Geochemistry, Genesis and Economic Aspect of Syenitic and Mafic Rocks in Mindif Complex, Far North Cameroon, Central Africa. *International Journal of Geosciences*, **10**, 1081-1114. https://doi.org/10.4236/ijg.2019.1012062

[5] Yang, J.H., Chung, S.L., Wilde, S.A., Wu, F., Chu, M.F., Lo, C.H. and Fan, H.R. (2005) Petrogenesis of Post-Orogenic Syenites in the Sulu Orogenic Belt, East China: Geochronological, Geochemical and Nd-Sr Isotopic Evidence. *Chemical Geology*, **214**, 99-125. https://doi.org/10.1016/j.chemgeo.2004.08.053

[6] Jimoh, M.T. and Raji, I.O. (2011) Economic Prospects of Nepheline Syenites Occurring around Awo, Southwestern, Nigeria. *Journal of Emerging Trends in Engineering and Applied Sciences* (*JETEAS*), **2**, 606-609.

[7] Demarco, M.M., Oyhantcabal, P., Stein, K.J. and Siegesmund, S. (2013) Granitic Dimensional Stones in Uruguay: Evaluation and Assessment of Potential Resources. *Environmental Earth Sciences*, **69**, 1397-1438.

[8] Lopes, L. (2017) Portuguese Dimension Stones: Sector Characterization and International Market Strategies. *Proceedings of the IV International Stone Congress*, Izmir, 20-25 March 2017, 47-62.

[9] Chiwona, A.G., Cortés, J.A., Gaulton, R.G. and Manning, D.A.C. (2020) Petrology and Geochemistry of Selected Nepheline Syenites from Malawi and Their Potential as Alternative Potash Sources. *Journal of African Earth Sciences*, **164**, Article ID: 103769. https://doi.org/10.1016/j.jafrearsci.2020.103769

[10] Jena, S.K., Dhawan, N., Rao, D.S., Misra, P.K., Mishra, B.K. and Das, B. (2014) Studies on Extraction of Potassium Values from Nepheline Syenite. *International Journal of Mineral Processing*, **133**, 13-22. https://doi.org/10.1016/j.minpro.2014.09.006

[11] Manning, D.A.C. (1995) Introduction to Industrial Minerals. Springer, Dordrecht. https://doi.org/10.1007/978-94-011-1242-0

[12] Bao, Z., Li, C. and Zhao, Z. (2016) Metallogeny of the Syenite-Related Dongping Gold Deposit in the Northern Part of the North China Craton: A Review and Synthesis. *Ore Geology Reviews*, **73**, 198-210. https://doi.org/10.1016/j.oregeorev.2015.04.002

[13] Bigot, L. and Jébrak, M. (2015) Gold Mineralization at the Syenite-Hosted Beattie Gold Deposit, Duparquet, Neoarchean Abitibi Belt, Canada. *Economic Geology*, **110**, 315-335. https://doi.org/10.2113/econgeo.110.2.315

[14] Legault, M. and Lalonde, A.E. (2004) Discrimination des syénites associées aux gisements aurifères de la sous-province de l'abitibi, Quebec, Canada. RP 2009-04 Quebec Government Publication, 10 p.

[15] Liu, Y. and Hou, Z. (2017) A Synthesis of Mineralization Styles with an Integrated Genetic Model of Carbonatite-Syenite-Hosted REE Deposits in the Cenozoic Mianning-Dechang REE Metallogenic Belt, the Eastern Tibetan Plateau, Southwestern China. *Journal of Asian Earth Sciences*, **137**, 35-79. https://doi.org/10.1016/j.jseaes.2017.01.010

[16] Mitchell, R.H., Platt, R.G., Lukosius-Sanders, J., Artist-Downey, M. and Moogk-Pickard, S. (1993) Petrology of Syenites from Center III of the Coldwell Alkaline Complex, Northwestern Ontario, Canada. *Canadian Journal of Earth Sciences*, **30**, 145-158. https://doi.org/10.1139/e93-014

[17] Gougazeh, M., Bamousa, A. and Hasan, A. (2018) Evaluation of Granitic Rocks as Feldspar Source: Al Madinah, Western Part of Saudi Arabia. *Journal of Taibah University for Science*, **12**, 21-36. https://doi.org/10.1080/16583655.2018.1451111

[18] Dias, F.G., Segadães, A.M., Perottoni, C.A. and Cruz, R.C.D. (2017) Assessment of the Fluxing Potential of Igneous Rocks in the Traditional Ceramics Industry. *Ceramics International*, **43**, 16149-16158. https://doi.org/10.1016/j.ceramint.2017.08.190

[19] Dondi, M. (2018) Feldspars and Other Fluxes for Ceramic Tiles: Sources, Processing, Composition and Technological Behavior. CRAM Raw Materials Profile, European Innovation Partnership on Raw Materials, 260 p.

[20] Elimbi, A., Dika, J.M. and Djangang, C.N. (2014) Effects of Alkaline Additives on the Thermal Behavior and Properties of Cameroonian Poorly Fluxing Clay Ceramics. *Journal of Minerals and Materials Characterization and Engineering*, **2**, 484-501. https://doi.org/10.4236/jmmce.2014.25049

[21] Hegazy, H.A., Arzamastsev, A.A. and Saad, E. (2016) Geology, Petrography and Geochemistry of El-kahfa Ring Complex, South Eastern Desert, Egypt. *Geochemistry*, **3**, 25-37.

[22] Ismail, A.I.M., Ghabrial, D.S., Wahab, W.A., Eissa, M., Cazzaniga, A., Zanelli, C. and Dondi, M. (2018) Exploring Syenites from Ring Complexes in the Eastern Desert (Egypt) as Ceramic Raw Materials. *Periodico di Mineralogia*, **87**, 67-81.

[23] Zahradník, J., Jirásek, J., Starý, J. and Sivek, M. (2020) Production, Reserves, and Processing of Feldspar and Feldspathoid Rocks in the Czech Republic from 2005 to 2019—An Overview. *Minerals*, **10**, Article No. 722. https://doi.org/10.3390/min10080722

[24] Zilles, J.U. (2013) Feldspar and Syenites. In: Palsule, S., Ed., *Encyclopedia of Polymers and Composites*, Springer, Berlin, 1-11. https://doi.org/10.1007/978-3-642-37179-0_5-5

[25] Njoya, D., Hajjaji, M., Nkoumbou, C., Elimbi, A., Kwekam, M., Njoya, A., Yvon, J. and Njopwouo, D. (2010) Chemical and Mineralogical Characterization and Ceramic Suitability of Raw Feldspathic Materials from Dschang (Cameroon). *Bulletin of the Chemical Society of Ethiopia*, **24**, 39-46. https://doi.org/10.4314/bcse.v24i1.52959

[26] Tchakounte Bakop, T., Tene Fongang, R.T., Melo, U.C., Kamseu, E., Miselli, P. and Leonelli, C. (2013) Sintering Behaviors of Two Porcelainized Stoneware Compositions Using Pegmatite and Nepheline Syenite Minerals. *Journal of Thermal Analysis and Calorimetry*, **114**, 113-123. https://doi.org/10.1007/s10973-012-2890-5

[27] Njimbouombouo, M.S., Yannick, O., Randy, C., André, N., Mouncherou, O. and Billong, N. (2020) Potential of Some Granites from Foumban (West Region of Cameroon) as Fluxing Materials for Ceramics. *Journal of Minerals and Materials Characterization and Engineering*, **8**, 353-363. https://doi.org/10.4236/jmmce.2020.85022

[28] Weecksteen, G. (1957) Carte géologique de reconnaissance du Cameroun à l'échelle 1/500 000. Levés effectués de 1949 à 1956. Notice explicative sur la feuille Douala-Est. Imp. Nat. Yaoundé.

[29] Tchindjang, P.M., Njilah, I.K., Nziengui, M. and Banga, C.R. (2006) Caractérisation par l'imagerie satellitale de trois grandes structures d'effondrement dans les hautes

terres de l'ouest cameroun. *African Journal of Science and Technology Science and Engineering Series*, **7**, 8-22.

[30] Kouankap, D.N.G., Wotchoko, P., Magha, A., Ganno, S., Njoya, N., Afahnwie Ngambu, A., Paul Nzenti, J. and Kamgang Kabeyene, V. (2018) Contrasting Ba-Sr Granitoids from Bamenda Area, NW Cameroon: Sources Characteristics and Implications for the Evolution of the Pan African Fold Belt. *Journal of Geosciences and Geomatics*, **6**, 65-76. https://doi.org/10.12691/jgg-6-2-4

[31] Toteu, S.F., Penaye, J. and Djomani, Y.P. (2004) Geodynamic Evolution of the Pan-African Belt in Central Africa with Special Reference to Cameroon. *Canadian Journal of Earth Sciences*, **41**, 73-85. https://doi.org/10.1139/e03-079

[32] Nzenti, J.P., Kapajika, B., Wörner, G. and Lubala, T.R. (2006) Synkinematic Emplacement of Granitoids in a Pan-African Shear Zone in Central Cameroon. *Journal of African Earth Sciences*, **45**, 74-86. https://doi.org/10.1016/j.jafrearsci.2006.01.005

[33] Nzenti, J.P. (1998) Neoproterozoic Alkaline Meta-Igneous Rocks from the Pan-African North Equatorial Fold Belt (Yaounde, Cameroon): Biotitites and Magnetite Rich Pyroxenites. *Journal of African Earth Sciences*, **26**, 37-47. https://doi.org/10.1016/S0899-5362(97)00135-8

[34] Ngako, V., Njonfang, E., Aka, F.T., Affaton, P. and Nnange, J.M. (2006) The North-South Paleozoic to Quaternary Trend of Alkaline Magmatism from Niger-Nigeria to Cameroon: Complex Interaction between Hotspots and Precambrian Faults. *Journal of African Earth Sciences*, **45**, 241-256. https://doi.org/10.1016/j.jafrearsci.2006.03.003

[35] Ngako, V., Affaton, P. and Njonfang, E. (2008) Pan-African Tectonics in Northwestern Cameroon: Implication for the History of Western Gondwana. *Gondwana Research*, **14**, 509-522. https://doi.org/10.1016/j.gr.2008.02.002

[36] Nguiessi, T.C., Nsifa, N., Tempieret, P. and Tchoua, F. (1997) Les granitoydes calco-alcalins, syn-cisaillement de Bandja dans la chaine panafricaine nord4quatoriale au Cameroun. *Comptes Rendus de l'Académie des Sciences—Series IIA—Earth and Planetary Science*, **325**, 95-101. https://doi.org/10.1016/S1251-8050(97)83969-9

[37] Dumont, J.F. (1986) Identification par télédétection de l'accident de la Sanaga (Cameroun): Sa position dans le contexte des grands accidents d'Afrique Centrale et de la limite nord du craton congolais. *Géodynamique*, **1**, 13-19.

[38] Njanko, T., Nédélec, A. and Affaton, P. (2006) Synkinematic High-K Calc-Alkaline Plutons Associated with the Pan-African Central Cameroon Shear Zone (W-Tibati Area): Petrology and Geodynamic Significance. *Journal of African Earth Sciences*, **44**, 494-510. https://doi.org/10.1016/j.jafrearsci.2005.11.016

[39] Nzina, A.C., Nzenti, J.P., Njiosseu, E.L.T., Ganno, S. and Ngnotue, T. (2010) Synkinematic Ferro-Potassic Magmatism from the Mekwene-Njimafofire Foumban Massif, along the Foumban-Banyo Shear Zone in Central Domain of Cameroon Pan-African Fold Belt. *Journal of Geology and Mining Research*, **2**, 142-158.

[40] Nzolang, C., Kagami, H., Nzenti, J.P. and Holtz, F. (2003) Geochemistry and Preliminary Data on the Neoproterozoic Granitoids from the Bantoun Area, West Cameroon: Evidence for a Derivation from a Paleoproterozoic to Archean Crust. *Polar Geoscience*, **16**, 196-226.

[41] Tanko, N.E.L., Nzenti, J.P., Njanko, T., Kapajika, B. and Nédélec, A. (2005) New U-Pb Zircon Ages from Tonga (Cameroon): Coexisting Eburnean-Transamazonian (2.1 Ga) and Pan-African (0.6 Ga) Imprints. *Comptes Rendus Geoscience*, **337**, 551-562. https://doi.org/10.1016/j.crte.2005.02.005

[42] Tchakounté, J., Eglinger, A., Toteu, S.F., Zeh, A., Nkoumbou, C., Mvondo-Ondoa,

J., Penaye, J., de Wit, M. and Barbey, P. (2017) The Adamawa-Yadé Domain, a Piece of Archaean Crust in the Neoproterozoic Central African Orogenic Belt (Bafia Area, Cameroon). *Precambrian Research*, **299**, 210-229. https://doi.org/10.1016/j.precamres.2017.07.001

[43] Tchameni, R., Pouclet, A., Penaye, J., Ganwa, A.A. and Toteu, S.F. (2006) Petrography and Geochemistry of the Ngaoundéré Pan-African Granitoids in Central North Cameroon: Implications for Their Sources and Geological Setting. *Journal of African Earth Sciences*, **44**, 511-529. https://doi.org/10.1016/j.jafrearsci.2005.11.017

[44] Ayonta Kenne, P., Tanko Njiosseu, E.L., Ganno, S., Ngnotue, T., Fossi, D.H., Hamdja Ngoniri, A., Nga Essomba, P. and Nzenti, J.P. (2021) Zircon Trace Element Geochemistry and Ti-in-Zircon Thermometry of the Linté Pan-African Granitoids, Central Cameroon: Constraints on the Genesis of Host Magma and Tectonic Implications. *Geological Journal*, **56**, 4830-4848. https://doi.org/10.1002/gj.4208

[45] Tchameni, R., Mezger, K., Nsifa, N.E. and Pouclet, A. (2001) Crustal Origin of Early Proterozoic Syenites in the Congo Craton (Ntem Complex), South Cameroon. *Lithos*, **57**, 23-42. https://doi.org/10.1016/S0024-4937(00)00072-4

[46] Toteu, S.F., Van Schmus, W.R., Penaye, J. and Michard, A. (2001) New U-Pb and Sm-Nd Data from North-Central Cameroon and Its Bearing on the Pre-Pan African History of Central Africa. *Precambrian Research*, **108**, 45-73. https://doi.org/10.1016/S0301-9268(00)00149-2

[47] Vicat, J.P., Moloto-A-Kenguemba, G.R. and Bilong, P. (1999) Les syénite de Monguélé (Sud-Est, Cameroun). In: Vicat, J.P. and Bilong, P., Eds., *Géologie et Environement du Cameroun*, Université de Yaoundé Press, Yaoundé, 387-396.

[48] Parsons, I., Fitz Gerald, J.D. and Lee, M.R. (2015) Routine Characterization and Interpretation of Complex Alkali Feldspar Intergrowths. *American Mineralogist*, **100**, 1277-1303. https://doi.org/10.2138/am-2015-5094

[49] Middlemost, E.A.K. (1994) Naming Materials in the Magma/Igneous Rock System. *Earth-Science Reviews*, **37**, 215-224. https://doi.org/10.1016/0012-8252(94)90029-9

[50] Irvine, T.N. and Baragar, W.R.A. (1971) A Guide to the Chemical Classification of the Common Volcanic Rocks. *Canadian Journal of Earth Sciences*, **8**, 523-548. https://doi.org/10.1139/e71-055

[51] Frost, B.R., Barnes, C.G., Collins, W.J., Arculus, R.J., Ellis, D.J. and Frost, C.D. (2001) A Geochemical Classification for Granitic Rocks. *Journal of Petrology*, **42**, 2033-2048. https://doi.org/10.1093/petrology/42.11.2033

[52] Barbarin, B. (1999) A Review of the Relationships between Granitoid Types, Their Origins and Their Geodynamic Environments. *Lithos*, **46**, 605-626. https://doi.org/10.1016/S0024-4937(98)00085-1

[53] Shand, S.J. (1943) Eruptive Rocks: Their Genesis, Composition, and Classification, with a Chapter on Meteorites. T. Murby & Co., London.

[54] Moyen, J.F. (2011) Eléments de nomenclature et quelques basespour comprendre et utiliser la classification des granitoïdes. Géologie de la Lorraine: Annexes scientifiques: Éléments de nomenclature et classification des granitoïdes. https://sites.ac-nancy-metz.fr/base-geol/annexe.php?id=22

[55] Omada, J.I., Kolawole, M.S. and Odoma, A.N. (2015) Field and Petrochemical Studies of Pegmatites in Parts of Lokoja, Central Nigeria. *Journal of African Earth Sciences*, **101**, 266-273. https://doi.org/10.1016/j.jafrearsci.2014.09.020

[56] Harker, A. (1909) The Natural History of Igneous Rocks. Methuen & Co., London.

[57] Marshall, D. (1996) Ternplot: An Excel Spreadsheet for Ternary Diagrams. *Computers & Geosciences*, **22**, 697-699. https://doi.org/10.1016/0098-3004(96)00012-X

[58] Whalen, J.B., Currie, K.L. and Chappell, B.W. (1987) A-Type Granites: Geochemical Characteristics, Discrimination and Petrogenesis. *Contributions to Mineralogy and Petrology*, **95**, 407-419. https://doi.org/10.1007/BF00402202

[59] Chappell, B.W. and White, A.J.R. (1974) I- and S-Type Granites in the Lachlan Fold Belt. *Earth and Environmental Science Transactions of the Royal Society of Edinburgh*, **83**, 1-26. https://doi.org/10.1017/S0263593300007720

[60] Barbarin, B. (1999) A Review of the Relationships between Granitoid Types, Their Origins and Their Geodynamic Environments. *Lithos*, **46**, 605-626.

[61] Pearce, J.A., Harris, N.B.W. and Tindle, A.G. (1984) Trace Element Discrimination Diagrams for the Tectonic Interpretation of Granitic Rocks. *Journal of Petrology*, **25**, 956-983. https://doi.org/10.1093/petrology/25.4.956

[62] Bonin, B. (2007) A-Type Granites and Related Rocks: Evolution of a Concept, Problems and Prospects. *Lithos*, **97**, 1-29. https://doi.org/10.1016/j.lithos.2006.12.007

[63] Rollinson, H. (1995) Using Geochemical Data: Evolution, Presentation, Interpretation. Longman Scientific and Technical Press, London.

[64] Burat, F., Kangal, O. and Onal, G. (2006) An Alternative Mineral in the Glass and Ceramic Industry: Nepheline Syenite. *Minerals Engineering*, **19**, 370-371. https://doi.org/10.1016/j.mineng.2005.10.015

[65] Mazhari, S.A., Hajalilou, B. and Bea, F. (2012) Evaluation of Syenite as Feldspar Source: Piranshahr Pluton, NW of Iran. *Natural Resources Research*, **21**, 279-283. https://doi.org/10.1007/s11053-012-9174-4

[66] Kangal, M.O., Bulut, G., Yeşilyurt, Z., Güven, O. and Burat, F. (2017) An Alternative Source for Ceramics and Glass Raw Materials: Augen-Gneiss. *Minerals*, **7**, Article No. 70. https://doi.org/10.3390/min7050070

[67] Potter, M.J. (2000) Feldspar and Nepheline Syenite. U.S. Geological Survey Minerals Yearbook, 6 p.

[68] Zanelli, C., Baldi, G., Dondi, M., Ercolani, G., Guarini, G. and Raimondo, M. (2008) Glass-Ceramic Frits for Porcelain Stoneware Bodies: Effects on Sintering, Phase Composition and Technological Properties. *Ceramics International*, **34**, 455-465. https://doi.org/10.1016/j.ceramint.2006.11.008

[69] Pantshi, B. and Theart, H.F.J. (2008) The Red Syenite of the Pilanesberg Complex; a Potential Raw Material Source for the South African Ceramics and Glass Industry. *South African Journal of Geology*, **111**, 27-38. https://doi.org/10.2113/gssajg.111.1.27

[70] Foucault, A. (2014) Le guide du géologue amateur. 2nd Edition, Dunod, Malakoff.

[71] Denïz, K. and Kadioğlu, Y.K. (2019) Investigation of Feldspar Raw Material Potential of Alkali Feldspar Granites and Alkali Feldspar Syenites within Central Anatolia. *Bulletin of the Mineral Research and Exploration*, **158**, 265-289. https://doi.org/10.19111/bulletinofmre.438197

[72] Arib, A., Sarhiri, A., Moussa, R., Remmal, T. and Gomina, M. (2007) Caractéristiques structurales et mécaniques de céramiques à base d'argiles: Influence de la source de feldspath. *Comptes Rendus Chimie*, **10**, 502-510. https://doi.org/10.1016/j.crci.2006.01.005

[73] Pouliquen, M. (2010) Les Feldspaths. Fiche détaillées lasim, 7 p.

[74] Amaireh, M. and Aljaradin, M. (2014) Characterization of the Jordanian Feldspar Raw Materials for Application in the Ceramic and Glass Industries. *International Journal of Mining Engineering and Mineral Processing*, **3**, 28-31.

[75] Celik, M.S., Pehlivanoglu, B., Aslanbas, A. and Asmatulu, R. (2001) Flotation of Colored Impurities from Feldspar Ores. *Mining, Metallurgy & Exploration*, **18**, 101-105. https://doi.org/10.1007/BF03402879

[76] Dogu, I. and Arol, A.I. (2004) Separation of Dark-Colored Minerals from Feldspar by Selective Flocculation Using Starch. *Powder Technology*, **139**, 258-263. https://doi.org/10.1016/j.powtec.2003.11.009

[77] El-Rehiem, F.H. and Abd El-Rahman, M.K. (2008) Removal of Colouring Materials from Egyptian Albite Ore. *Mineral Processing and Extractive Metallurgy*, **117**, 171-174. https://doi.org/10.1179/174328508X272371

[78] Silva, J.C., Ulsen, C., Bergerman, M.G. and Horta, D.G. (2019) Reduction of Fe_2O_3 Content of Foyaite by Flotation and Magnetic Separation for Ceramics Production. *Journal of Materials Research and Technology*, **8**, 4915-4923. https://doi.org/10.1016/j.jmrt.2019.06.017

[79] Abdel-Khalek, N.A., Yehia, A. and Ibrahim, S.S. (1994) Technical Note Beneficiation of Egyptian Feldspar for Application in the Glass and Ceramics Industries. *Minerals Engineering*, **7**, 1193-1201. https://doi.org/10.1016/0892-6875(94)90006-X

[80] Gaied, M.E. and Gallala, W. (2015) Beneficiation of Feldspar Ore for Application in the Ceramic Industry: Influence of Composition on the Physical Characteristics. *Arabian Journal of Chemistry*, **8**, 186-190. https://doi.org/10.1016/j.arabjc.2011.04.011

[81] Orhan, E.C. and Bayraktar, İ. (2006) Amine-Oleate Interactions in Feldspar Flotation. *Minerals Engineering*, **19**, 48-55. https://doi.org/10.1016/j.mineng.2005.06.001

[82] Demir, C., Karagüzel, C., Gülgönül, I. and Çelik, M.S. (2004) Selective Separation of Sodium and Potassium Feldspar Minerals from Orebodies. *Key Engineering Materials*, **264-268**, 1435-1438. https://doi.org/10.4028/www.scientific.net/KEM.264-268.1435

[83] Karaguzel, C., Gulgonul, I., Demir, C., Cinar, M. and Celik, M.S. (2006) Concentration of K-Feldspar from a Pegmatitic Feldspar Ore By Flotation. *International Journal of Mineral Processing*, **81**, 122-132. https://doi.org/10.1016/j.minpro.2006.07.008